AGU PUBLICATIONS

JGR

Journal of Geophysical Research: Atmospheres

RESEARCH ARTICLE
10.1002/2017JD027033

Key Points:
- WRF 4 km simulations over two seasons realistically captured observed MCS statistics and large-scale environments in the central United States
- The longest-lived MCSs occur just ahead of westerly troughs and feedback to the environment through diabatic heating
- The long-lived MCSs produce a midlevel circulation anomaly that maintains the MCS and strengthens the environmental trough

Correspondence to:
L. R. Leung,
ruby.leung@pnnl.gov

Citation:
Yang, Q., Houze, R. A., Jr, Leung, L. R., & Feng, Z. (2017). Environments of long-lived mesoscale convective systems over the central United States in convection permitting climate simulations. *Journal of Geophysical Research: Atmospheres*, *122*, 13,288–13,307. https://doi.org/10.1002/2017JD027033

Received 26 APR 2017
Accepted 5 DEC 2017
Accepted article online 12 DEC 2017
Published online 28 DEC 2017

©2017. American Geophysical Union. All Rights Reserved.
This manuscript has been authored by Battelle Memorial Institute under contract number DE-AC05-76RL01830 with the U.S. Department of Energy. The United States Government retains and the publisher, by accepting this article for publication, acknowledges that the United States Government retains a nonexclusive, paid-up, irrevocable, worldwide license to publish or reproduce the published form of this manuscript, or allow others to do so for United States Government purposes. The Department of Energy will provide public access to these results of federally sponsored research in accordance with the DOE Public Access Plan: (http://energy.gov/downloads/doe-public-access-plan).

Environments of Long-Lived Mesoscale Convective Systems Over the Central United States in Convection Permitting Climate Simulations

Qing Yang[1], Robert A. Houze Jr[1,2], L. Ruby Leung[1], and Zhe Feng[1]

[1]Atmospheric Sciences and Global Change Division, Pacific Northwest National Laboratory, Richland, WA, USA, [2]Department of Atmospheric Sciences, University of Washington, Seattle, WA, USA

Abstract Continental-scale convection-permitting simulations of the warm seasons of 2011 and 2012 using the Weather Research and Forecasting model reproduce realistic structure and frequency distribution of lifetime and event mean precipitation of mesoscale convective systems (MCSs) over the central United States. Analysis is performed to determine the environmental conditions conducive to generating long-lived MCSs. The simulations show that MCSs systematically form over the central Great Plains ahead of a trough in the westerlies in combination with an enhanced low-level moist jet from the Gulf of Mexico. These environmental properties at the time of storm initiation are most prominent for the MCSs that persist for the longest times. MCSs reaching lifetimes of 9 h or more occur closer to the approaching trough than shorter-lived MCSs. These long-lived MCSs exhibit the strongest feedback to the environment through diabatic heating in the trailing regions of the MCSs. The feedback strengthens the synoptic-scale trough associated with the MCS by producing an anomaly circulation characterized by a divergent perturbation at high levels over the MCS and a midlevel cyclonic circulation perturbation near the trough line in association with the trailing portion of the MCS. The quasi-balanced mesoscale vortex may help to maintain the MCS over a long period of time by feeding dry, cool air into the environment at the rear of the MCS region that enhances evaporative cooling and helps maintain the MCS.

1. Introduction

A mesoscale convective system (MCS) is a contiguous cumulonimbus cloud complex with horizontal dimensions of hundreds to a few thousand kilometers and lasts up to ~10–24 h. Comprehensive reviews of this type of convective storm have been provided by Fritsch and Forbes (2001) and Houze (2004) and are included in various textbooks (e.g., Cotton et al., 2011; Houze, 2014; Markowski & Richardson, 2010). MCSs occur in both tropics and middle latitudes and have gone by various names in the literature. In the tropics they were referred to as "cloud clusters" in the earliest work (Frank, 1970; Houze & Betts, 1981; Martin & Suomi, 1972). One subclass of MCSs that has received much attention is the "squall line" in which the active convective elements occur in the form of a leading line of active cumulonimbus connected to a trailing region of stratiform cloud and precipitation (Hamilton et al., 1945; Houze, 1977; Rotunno et al., 1988; Zipser, 1969, 1977; and many others). Many MCSs, however, have the active convective cells and stratiform regions arranged in more complex patterns (e.g., Houze et al., 1990; Leary & Houze, 1979). Maddox (1980) focused attention on a very intense form of MCSs, the so-called mesoscale convective complex, or MCC, identifiable in infrared satellite imagery as having a large, cold cloud top ($\geq 10^5$ km^2, brightness temperature $\leq$ 241 K, with interior cold cloud center of brightness temperature $\leq$ 221 K exceeding an area of 5×10^4 km^2) of roughly circular shape.

MCSs are important precipitation producers, accounting for 30–70% of warm season rainfall in the region between the Rocky Mountains and Mississippi River (Fritsch et al., 1986) and some 50–60% of tropical rainfall (Yuan & Houze, 2010). From well-developed MCSs some 40% of the precipitation is stratiform (e.g., Cheng & Houze, 1979; Chong & Hauser, 1989; Gamache & Houze, 1982; Rutledge & Houze, 1987). The combination of convective and stratiform rain in an MCS can lead to extended periods of rainfall and sometimes flooding at particular locations (e.g., Rasmussen et al., 2015). Not only do MCSs tend to produce floods but they also carry with them a variety of attendant severe weather phenomena (Houze et al., 1990). The role of MCSs in the water cycle is thus important on both short and long timescales. Feng et al. (2016) have shown that observed increases in springtime total and extreme rainfall in the central United States in the past 35 years are dominated by increased frequency and intensity of long-lasting MCSs. Investigation of the environmental

conditions producing long-lived MCSs is therefore a priority in determining how heavy precipitation events might change in character and location in a changing climate. Such investigations will require that the relationships between MCSs and their large-scale environment be reasonably captured by climate models used to project future changes.

The connections of MCSs to larger scales of motion are both important and not fully understood. The first article on cloud clusters by Frank (1970) was concerned with trying to relate them to synoptic-scale easterly waves in the tropics. Fragments of evidence since that time suggest a synergy between the larger-scale disturbances and MCSs. Over tropical oceans, MCSs are found to maximize their frequency in harmony with the upward motion sectors of equatorial waves (e.g., Payne & McGarry, 1977; Zuluaga & Houze, 2013). In their "building block" concept, Mapes et al. (2006) hypothesized that tropical MCSs reach lifecycle stages in the portions of waves most supportive of those stages. For midlatitude continental convection, Maddox (1983) used composites of sounding data around MCCs to show that over the central United States MCCs are linked to synoptic-scale troughs in the westerlies, with storms initiating ahead of troughs, where large-scale lifting occurs. Peters and Schumacher (2014) composited large-scale atmospheric environments associated with heavy rain producing MCSs using reanalysis product. They found that warm-season MCSs often occur near the entrance region of an upper-level jet and strong low-level warm and moist air advection from the southwest. Carbone et al. (2002) showed further that MCSs over the central United States systematically rejuvenate in an eastward progression suggestive of a subsynoptic propagating wave-like mechanism favoring successive regeneration of MCSs. Coniglio et al. (2010) identified key elements including the nocturnal low-level jet, frontal zone, moisture profile, and wind shear that distinguish the longevity of MCSs in the central United States. Laing and Fritsch (2000) found that the dynamical and thermodynamical environments of MCCs in the United States are also present in other MCC population centers around the world. These various studies indicate that both synoptic and subsynoptic motion systems link with MCS behavior, but the nature of the scale interactions in that linkage remains incompletely understood.

While Maddox (1983) established that region ahead of the trough of a wave in the westerlies is a favorable condition for MCCs (and undoubtedly MCSs in general), there is further evidence that MCSs positively reinforce their parent large-scale circulations. It is thought that the heating mechanisms in longer-lived MCSs are a pathway for upscale interaction. The stratiform regions develop a midlevel cloud base with updraft and heating above and cooling by evaporation and melting below (Houze, 1982, 1989). Processes in the stratiform region thus make the MCS heating profile top heavy, providing generation of potential vorticity (proportional to the vertical gradient of heating) in midlevels (Fritsch et al., 1994). Many observations are consistent with this potential vorticity (PV) generation: Gamache and Houze (1985) found that a tropical oceanic MCS developed cyclonic circulation in midlevels in its stratiform region. Bartels and Maddox (1991) showed also that long-lived MCSs in midlatitudes frequently develop persistent "mesoscale convective vortices (MCVs)."

The potential vorticity generation by MCSs impacts the large-scale circulation in which the cloud systems are embedded. Therefore, the longer lived an MCS, the greater will be its feedback effect on the large-scale flow. An important question is, what constitutes a long-lived MCS? Fritsch and Forbes (2001) noted that it takes about 3–6 h for Coriolis influences to become significant in an MCS. Also, Cotton et al. (1989) showed that midlatitude MCSs ~300 km or more in horizontal scale are comparable to or larger than the Rossby radius, implying that the wind and mass fields of the MCS are quasi-balanced. Davis et al. (2002) noted that MCVs can be simulated once balanced circulations are established, but that models have virtually no skill in predicting the formation of MCVs 12 h in advance. A long-lived quasi-balanced MCS traps energy locally so it can be absorbed by and modify the parent synoptic-scale circulation. As a result, the enhanced positive potential vorticity of the MCS can make the parent large-scale trough stronger and more capable of supporting further occurrences of MCSs. These considerations suggest that in the context of climate modeling, the most challenging MCSs to represent are those exceeding 300 km in horizontal scale and lasting more than 6 h. Capturing the dynamics of the large-scale environment that supports such MCSs is thus crucial for preventing model errors in predictions of the future course of the large-scale circulation. As long-lived MCSs are important for precipitation (Doswell et al., 1996), understanding the large-scale environment of long-lived MCSs is also important for predicting water cycle changes in regions dominated by MCSs.

A variety of evidence indicates that the upscale feedbacks of MCSs are indeed important to the large-scale circulation. In the tropics, the mean planetary-scale circulation driven by heating near the equator takes on a more realistic structure when the vertical profile of heating in regions of precipitation is assumed to be increasingly top heavy in proportion to the stratiform precipitation fraction associated with deep convection (Hartmann et al., 1984; Schumacher et al., 2004). The active phase of the Madden-Julian Oscillation is coincident with top-heavy heating profiles in the stratiform regions of MCSs (Barnes et al., 2015). In midlatitudes, cumulative effects of persistent intense MCSs also produce significant changes in the large-scale flow. Stensrud (1996) used a hydrostatic model with parameterized convection (nested grid down to 30 km spacing) to show that in regions of persistent deep convection (1) low-level warm moist flow is enhanced, increasing the likelihood that such convection will continue; (2) at midlevels strengthening of the low-level baroclinity modifies the phase relationship between pressure and thermal waves; and (3) at upper levels anticyclonic perturbation of the flow by the convection acts as a source region of traceable Rossby waves. Although the convection was parameterized and cannot be specifically associated with MCSs, Stensrud's (1996) results point to the importance of long-lived convective systems as being the ones most likely to engender upscale feedback. The feedback from MCSs to the circulation could occur via potential vorticity generated by diabatic heating associated with precipitation produced by the MCSs. Raymond and Jiang (1990) and Li and Smith (2010) found that convectively generated potential vorticity projects favorably onto the first baroclinic gravity wave mode and plays an important role in spawning organized convective events. Comparing climate simulations with and without embedded explicit convection, Pritchard et al. (2011) found that the heating-atop-cooling profile associated with convection is key to generating organized propagating convection or MCSs. Trier et al. (2006) studied a single long-lived episode of successive propagating nocturnal convection using an explicit convection simulation at 4 km grid spacing over the central United States.

It follows from all the above considerations that prediction of especially long-lived MCSs will be crucial to understanding future changes in the water cycle. Also, MCSs are not passive riders on the large-scale flow; not only are they key elements in the occurrence of major precipitation events but they are also inextricably entwined in any change of the global circulation such that they influence how the large-scale circulation promotes future MCS events. From such close association of long-lived MCSs with large-scale circulation dynamics and water cycle, it follows that assessment of the role of long-lived MCSs in a changing climate depends on (1) assessing the ability of models to simulate long-lived MCSs and capture their relationships with the large-scale environment and (2) gaining a better understanding of the large-scale environmental conditions and potential feedbacks that favor long-lived MCSs. Previous studies of potential changes in midlatitude severe convective patterns as synoptic environments evolve have focused on how stability, wind shear, and moisture conditions will change under greenhouse warming (Diffenbaugh et al., 2013) and how the occurrence of tornadic storms will be affected (Trapp & Hoogewind, 2016). In this study, we use model simulations conducted over warm seasons to examine specifically how MCSs interact with synoptic-scale environmental conditions so that climate projections of changing synoptic conditions will apply more specifically to MCSs.

In contrast to Coniglio et al. (2010), who used observed precipitation to identify MCSs and analyzed large-scale circulation at 20 km grid spacing with parameterized convection, we pursue our goal by evaluating MCS statistics simulated by a convection-permitting model and using the simulations covering the warm seasons to provide a comprehensive set of results depicting MCSs and their interactions with the large-scale environments. Specifically, we use continental-scale, season-long convection-permitting simulations at 4 km grid spacing. Adopting a similar configuration, Gao et al. (2017) showed significant improvement in simulating the diurnal variability and propagation of cloud and precipitation in the central United States compared to simulations at 12 km and 36 km resolution with cumulus parameterizations. Liu et al. (2016) also demonstrated good performance of continental-scale convection-permitting simulations in capturing seasonal and subseasonal precipitation in North America. These simulations are consistent with the results of Weisman et al. (1997), who found that a resolution of 4 km is sufficient for simulating squall lines in the midlatitude environments. Applying a satellite-tracking method to observations and the model simulations, we first demonstrate the model fidelity in producing a climatology of MCS characteristics such as lifetime over the central United States. Then using model outputs from the simulations, we perform analysis to determine the environmental conditions conducive to generating the longest-lived MCSs and their subsequent interactions.

2. Model Simulations, Analysis Methods, and Observations

2.1. Model Configuration

Simulations in this study have been carried out with version 3.6.1 of the Weather Research and Forecasting (WRF) model (Skamarock et al., 2008) with the YSU planetary boundary layer scheme (Hong et al., 2006), the two-moment cloud microphysical scheme of Morrison et al. (2009), and the Rapid Radiative Transfer Model (Mlawer et al., 1997) and Goddard formulation (Chou & Suarez, 1994) for longwave and shortwave radiative transfer, respectively. An equivalent radar reflectivity factor was calculated with a simulator for S band (10 cm wavelength) radar with the hydrometeor mixing ratios simulated by the microphysics parameterization as input. The horizontal grid spacing was 4 km, and 65 vertical layers from the surface to 50 hPa were used. The domain covered most of the contiguous United States from about 28°N to 50°N and 120°W to 70°W. The simulations were conducted for two warm seasons: 1 May to 31 August 2011 and 1 May to 31 August 2012. Global Forecast System reanalysis data provided initial and lateral boundary conditions. Simulations were carried out by integrating over the 4 month periods beginning at 0600 UTC 1 May 2011 (reanalysis data missing for 0000 UTC) and 0000 UTC 1 May 2012). Note that 2012 was an anomalously dry summer over the Great Plains with lower frequency of MCSs (Pinto et al., 2015), so the two summers of 2011 and 2012 provide a useful contrast. Model output was archived at an hourly frequency.

2.2. Composites of Model Output

To determine the conditions associated with long-lived MCSs, we constructed two types of composites of the model output.

Geographically fixed composites: Two subtypes of geographically fixed composites were constructed.

1. No MCS occurrence (denoted "noMCS" in figures shown later) is defined as no MCS existing within 6 h over the central United States in an area bounded by 30–44°N and 83–110°W (shown in a later figure). A total of 274 hourly outputs from 8 months of simulation data is identified as noMCS.
2. MCS initiation (denoted "initMCS" in figures shown later) is defined as the time of first detection of deep convective cells or connected cold-cloud shield pixels that later develop into an MCS. The cold-cloud shield at the time of initiation is not required to meet the size criterion of an MCS. The region considered for storm initiation (shown in later figures) is confined to a zone over the Southern Great Plains (SGP), which is east of the Rocky Mountains and bounded by 32°–42°N and 96°W–102°W. The zone is limited to this region to avoid compositing synoptic conditions over regions with very different climatological conditions. Since the composites at 6 h and 3 h prior to an MCS initiation (referred to as -6 h and -3 h, respectively) and at the time of an initiation (0 h) show very similar synoptic features, we averaged the composite fields of -3 h and 0 h, resulting in 49 hourly outputs for 18 MCS initiations over the SGP.

Relative-location composites: The relative-location composites are useful for analysis of mesoscale features related to the MCS development. They are constructed as follows.

1. The meteorological variables were composited over a moving box (301 × 201 grid elements or ~13° longitude × 7° latitude). The center of the box was located at the geometric centroid of the storm complex at 0, +3, +6, and +9 h. The geometric centroid was determined as the center of mass of the contiguous cold-cloud shield. Composites for -6 and -3 h were also developed based on the centroid of the storm at 0 h. We included only MCSs that initiate within the region between 30°–47°N and 102°W–86°W and last at least 6 h. The MCS composite was divided into three categories, short, medium, and long lived, corresponding to MCS lifetime (t): $t < 9$ h, 9 h $\leq t < 18$ h, and $t \geq 18$ h, respectively. This procedure resulted in 49, 57, and 46 short-, medium-, and long-lived systems, respectively.

The anomalies analyzed in this study were calculated for each grid box as the deviation from the corresponding time mean value over the grid calculated for each hour of the day and for each month to remove the mean seasonal and diurnal variations. Variables with a height dimension, such as geopotential height, were composited on five fixed pressure surfaces at 900, 850, 700, 500, and 300 hPa.

2.3. Observations Used to Evaluate the Simulations

Gridded radar reflectivity over the United States: The National Severe Storms Laboratory National Mosaic and Multi-Sensor Quantitative Precipitation Estimation (NMQ) 3-D Reflectivity Mosaic data are based on objectively merged multiradar measurements from the Weather Surveillance Radar 1988 Doppler (WSR-88D)

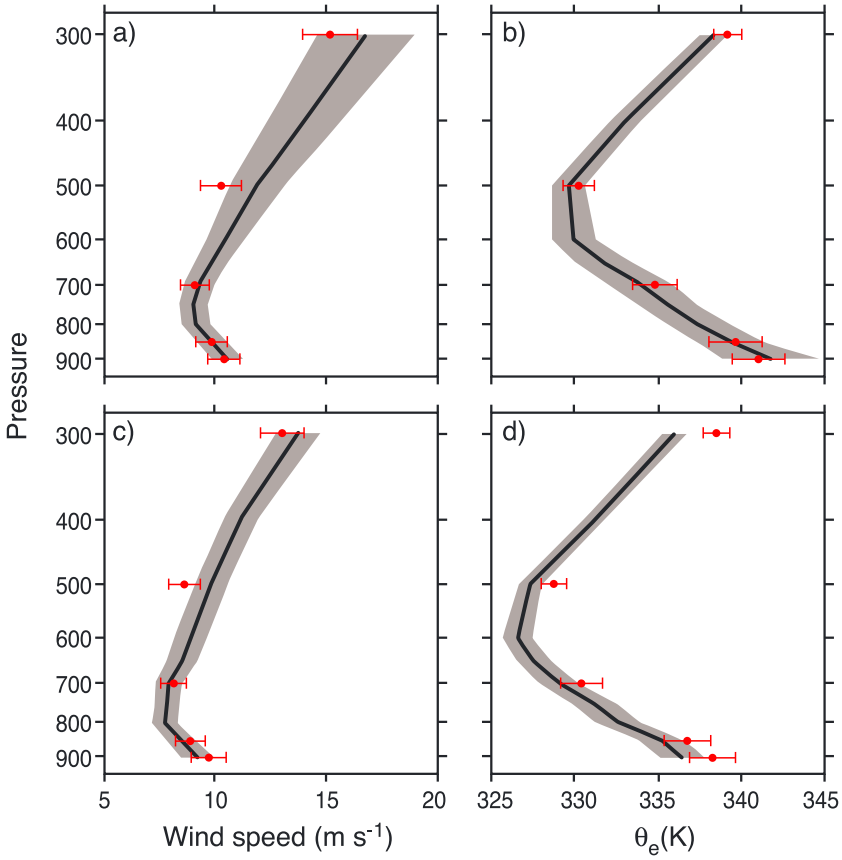

Figure 1. Comparison of radiosonde measured (red dots and bars) and WRF simulated (black lines and shading) wind speed and equivalent potential temperature (θ_e) over the ARM SGP central facility (97.49°W, 36.61°N) during May–August (a, b) 2011 and (c, d) 2012, respectively, at a 6 h frequency. The wind speed is based on 368 and 333 profiles for 2011 and 2012, respectively, and the θ_e is based on 220 and 196 profiles for 2011 and 2012, respectively. The red bars and shaded areas correspond to one standard deviation on each side of the measured and simulated values.

network (J. Zhang et al., 2011). The reflectivity data have a uniform grid size of 0.01° latitude × 0.01° longitude and 31 vertical levels from 0.5 km to 18 km. The NMQ data were averaged to a grid spacing of 4 km before applying an MCS tracking algorithm for comparison with the model simulations.

Gridded rainfall data: Two sets of precipitation data were used. One was from the North America Land Data Assimilation Systems (NLDAS) meteorological forcing data set (http://ldas.gsfc.nasa.gov/nldas/NLDAS2forcing.php#AppendixC). The NLDAS precipitation estimates combine ground-based gridded rain gauge analysis, radar, and satellite observations over the continental United States into a uniform hourly 1/8th degree (~12 km) resolution data product. The NLDAS daily total precipitation amount is the same as the daily rain gauge-only Climate Prediction Center (CPC) gridded precipitation analysis, and the disaggregation of the CPC daily total rainfall into hourly rainfall is based on hourly temporal weights obtained from the radar/satellite remote sensing precipitation. The other precipitation product was provided as part of the NMQ product. The NMQ hourly accumulation precipitation used in this study is based on radar estimates only. The NMQ precipitation product is provided on the same 0.01° latitude × 0.01° longitude grid as the NMQ radar reflectivity, and it was also averaged to a 4 km grid spacing in this study.

Satellite brightness temperature: The global satellite 11.5 μm infrared (T_{IR}) brightness temperature data set used in this study is produced by the CPC and National Centers for Environmental Prediction as a NASA Tropical Rainfall Measurement Mission ancillary data set (Janowiak et al., 2001). The primary geostationary satellite over the study domain is the Geostationary Operational Environmental Satellite-East. The T_{IR} data set has a 30 min temporal resolution and approximately 4 km × 4 km spatial resolution.

Sounding data: Vertical profiles of humidity and temperatures were obtained from the regular radiosonde observations over the Southern Great Plains (SGP) at the Atmospheric Radiation Measurement (ARM)

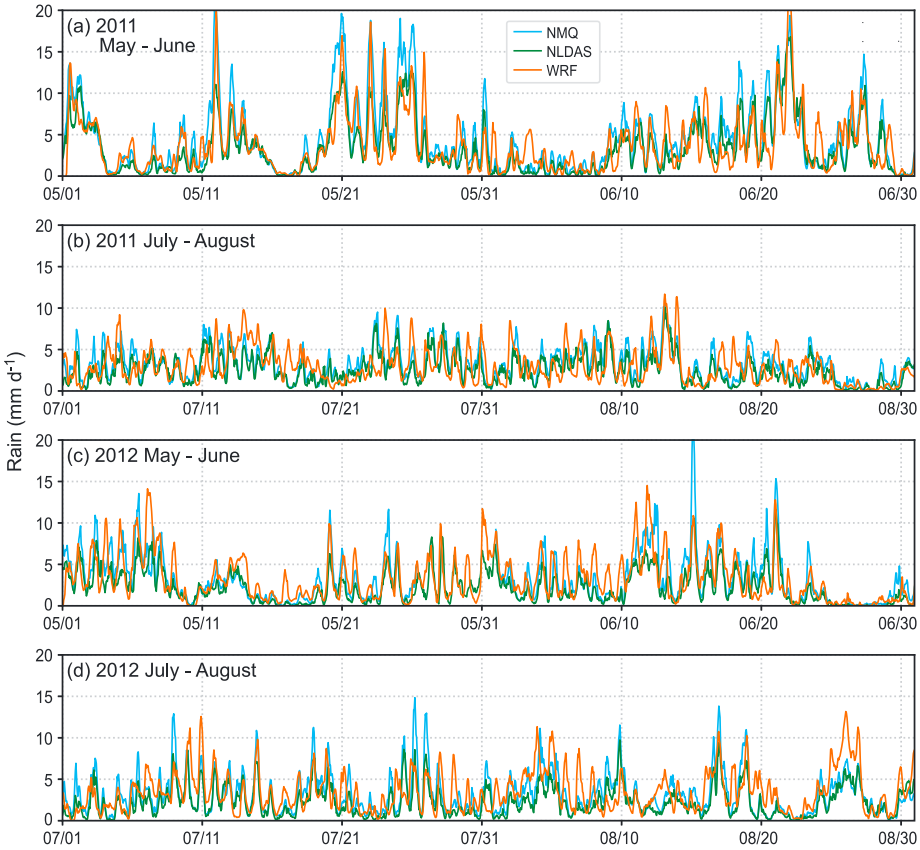

Figure 2. Time series of surface precipitation rate (in mm d^{-1}) from radar (NMQ), NLDAS (NLD), and model simulations (WRF) averaged over the central United States., roughly from 102°W to 84°W and 31°N to 48°N, inside the WRF domain for May–August, (a, b) 2011 and (c, d) 2012.

Climate Research central facility (Coulter et al., 1994). The radiosondes were released at a 6 h frequency, with enhanced 3 h frequency during the Midlatitude Continental Convective Cloud Experiment (Jensen et al., 2016) between April and May 2011.

2.4. MCS Tracking

An automated cloud-tracking method (Feng et al., 2012; Hagos et al., 2013) was applied to the satellite T_{IR} data set to track convective cloud systems. The tracking method identifies deep convection as contiguous satellite pixels with $T_{IR} \leq 241$ K and designates them as cold cloud shields. Convective clouds with a cold cloud shield are then tracked throughout their lifetime. Following the definition by Fritsch et al. (1986) and Kane et al. (1987), a cloud system with its cold cloud shield area exceeding 6×10^4 km^2 that persists at least 4 h is identified as an MCS. This definition is consistent with previous satellite-based definitions of MCCs and MCSs (e.g., Feng et al., 2016; Maddox, 1980; Nesbitt et al., 2000; Yuan & Houze, 2010). The model-simulated outgoing longwave radiation at the top model layer was first converted to equivalent T_{IR} following the formula proposed by Yang and Slingo (2001) (their equation (1)). Then the same cloud-tracking method was applied to the model's equivalent T_{IR} to identify MCSs.

3. Model Evaluation

The model-simulated vertical profiles of wind speed and equivalent potential temperature (θ_e) are compared against the 3-hourly coincident radiosonde observations over the ARM SGP central facility (Figure 1). The simulated mean wind speed at the five pressure levels (900, 850, 700, 500, and 300 hPa) of the composites agree well with the radiosonde observations with no statistically significant differences at a 0.025 significance level in both warm seasons (May–August in 2011 and 2012). The mean simulated θ_e also generally agrees with the observations at all five pressure levels but with an ~2–3°C cold bias in 2012.

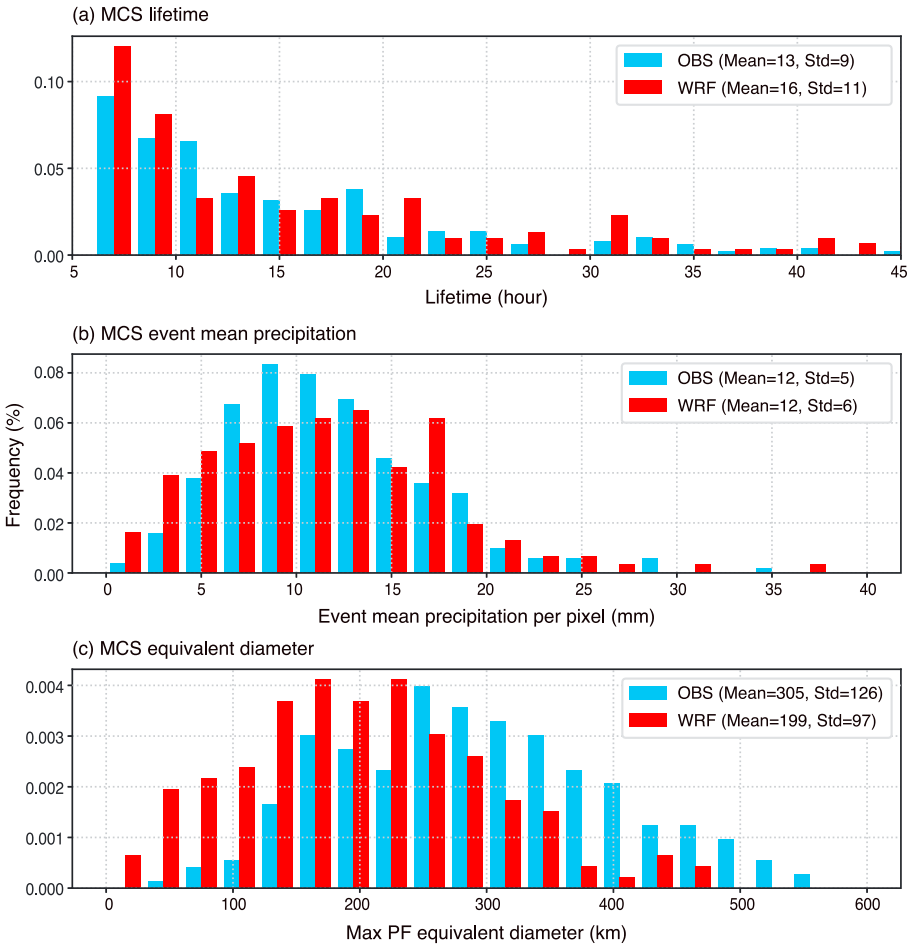

Figure 3. Comparision of simulated (WRF) and observed (OBS) frequency distribution of (a) MCS lifetime, (b) event mean precipitation per pixel, and (c) equivalent diameter of the MCS precipitation feature. The MCS event mean precipitation is the event accumulated precipitation averaged over the pixels that precipitate due to a particular MCS event is detected based on the NMQ or simulated precipitation.

That difference has no bearing on the conclusion of this study. The mean wind speed and θ_e are noticeably smaller in 2012 than 2011 throughout the atmosphere, with the smaller θ_e related to colder and drier mean conditions.

The simulated precipitation correlates well temporally with the hourly observationally based precipitation averaged over an area east of the Rockies within the WRF domain (correlation coefficient = 0.71 for 2011 and 0.61 for 2012; Figure 2). The averaging area covers roughly from 102°W to 84°W and 31°N to 48°N that is frequented by MCSs. The correlation coefficients between the model and the NLDAS hourly domain-averaged data are comparable (0.72 for 2011 and 0.66 for 2012). However, the model simulated comparable precipitation between 2011 (3.38 mm d^{-1}) and 2012 (3.40 mm d^{-1}), while the radar-derived and NLDAS precipitation is obviously higher in 2011 (3.91 mm d^{-1} and 2.91 mm d^{-1}) than 2012 (3.22 mm d^{-1} and 2.30 mm d^{-1}). Uncertainty in the observations is also significant as the NLDAS precipitation is notably lower than the radar-derived precipitation.

Figure 3 compares the probability density functions (PDFs) of MCS lifetime, event mean precipitation per pixel (4 km × 4 km), and the maximum equivalent diameter of the MCS precipitation feature for both observations and model simulations for the 8 months analyzed. Event mean precipitation per pixel is calculated as follows: pixels underneath the tracked cold-cloud shield recording more than 1 mm h^{-1} precipitation are included to calculate the accumulated precipitation throughout an MCS event; all the pixels that record more than 1 mm rainfall accumulation are then averaged to obtain event mean precipitation for each MCS. The simulated and observed MCS lifetime PDFs are generally similar, with a slightly

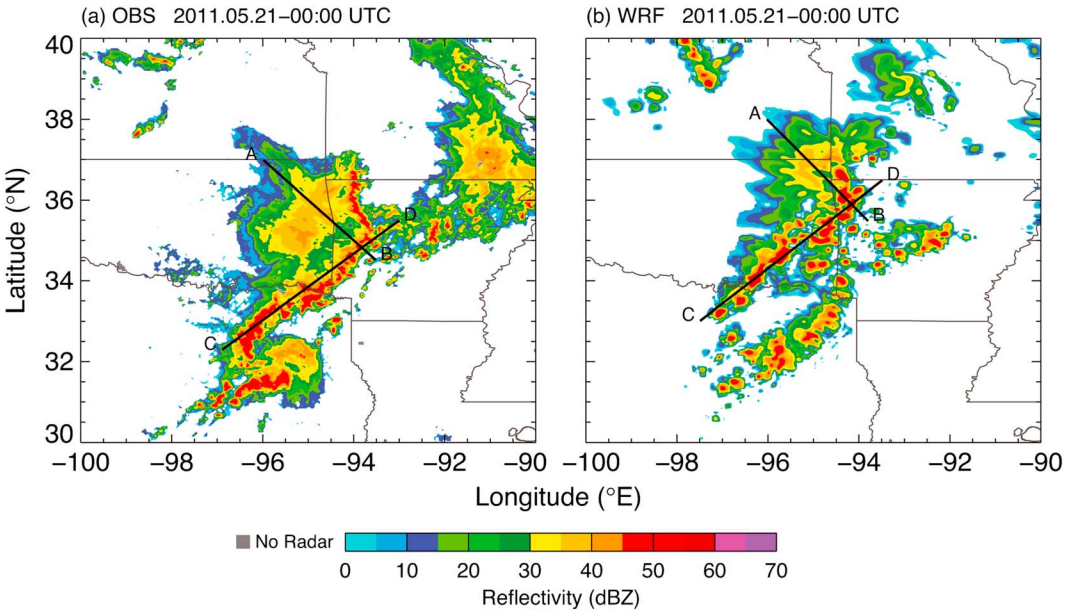

Figure 4. (a) Observed and (b) simulated radar reflectivity at the 2.5 km (AGL) level during an MCS event at 0000 UTC 21 May 2011.

shorter mean lifetime in the observations than simulations (13 versus 16 h; Figure 3a). The majority of MCSs did not exceed 24 h in lifetime. A limited number of MCSs lasting longer than 24 h in both observations and model simulations were caused by merging of two or more MCSs. These merging MCSs may have more complicated processes involved and are excluded from our current analysis. A very small number of MCSs that lasted longer than 24 h were not associated with merging so they were included in the composite analyses to increase the sample size, but their impacts should be small because the composite analysis focuses mainly on the period between convective initiation and 9 h after initiation. The PDFs of the observed and simulated MCS event mean precipitation per pixel also agree reasonably well, and the means are identical at 12 mm for observations and simulations (Figure 3b). However, the model tends to overestimate the frequency of both lightly and heavily precipitating MCSs and to underestimate the frequency of MCS with moderate precipitation intensity. As a result, the PDF for the model cases is slightly broader (as seen from higher standard deviation). As shown in Figure 3c, the model overestimates the frequency of the small-sized MCSs ($<$ 250 km) and underestimates the frequency of large-sized MCSs ($>$ 250 km), as measured by the equivalent diameter of the precipitation feature. The short- and medium-lived MCSs have similar mean diameter of about 180 km, but the long-lived MCSs are notably larger with a mean diameter of ~275 km. The size variations within each category of MCSs are small relative to the mean diameter.

To demonstrate how well the simulations at 4 km grid spacing capture the internal structure of the storms, Figure 4 shows the 21 May 2011 case, which was a typical large and long-lived MCS. The observed horizontal radar reflectivity pattern at a height of 2.5 km in Figure 4a is similar to that of the corresponding simulated structure in Figure 4b. This altitude is below the melting level and therefore unaffected by the bright band. The observed radar echo shows a stratiform region centered along line AB and a convective line along line CD. The precipitation area was moving eastward, and the juxtaposition of convective line and stratiform region was typical of an MCS categorized as "asymmetric" by Houze et al. (1990). As is typical of convection-permitting models using bulk microphysics parameterizations (see, e.g., the discussion in Houze, 2014, Chapter 9), the area of stratiform precipitation is underestimated by the model. The positioning of the MCS is about 1° off to the north. Such errors in location shift are likely related to the experimental setup for continuous rather than short-term simulations and should have no significant effect on the composited and statistical results that we focus on in this study. The underestimation of the stratiform regions may produce a bias due to underestimation of the diabatic effects of stratiform cloud and precipitation. As will be shown below, even with this possible underestimation, the imprint of stratiform region physics and dynamics on the results is strong.

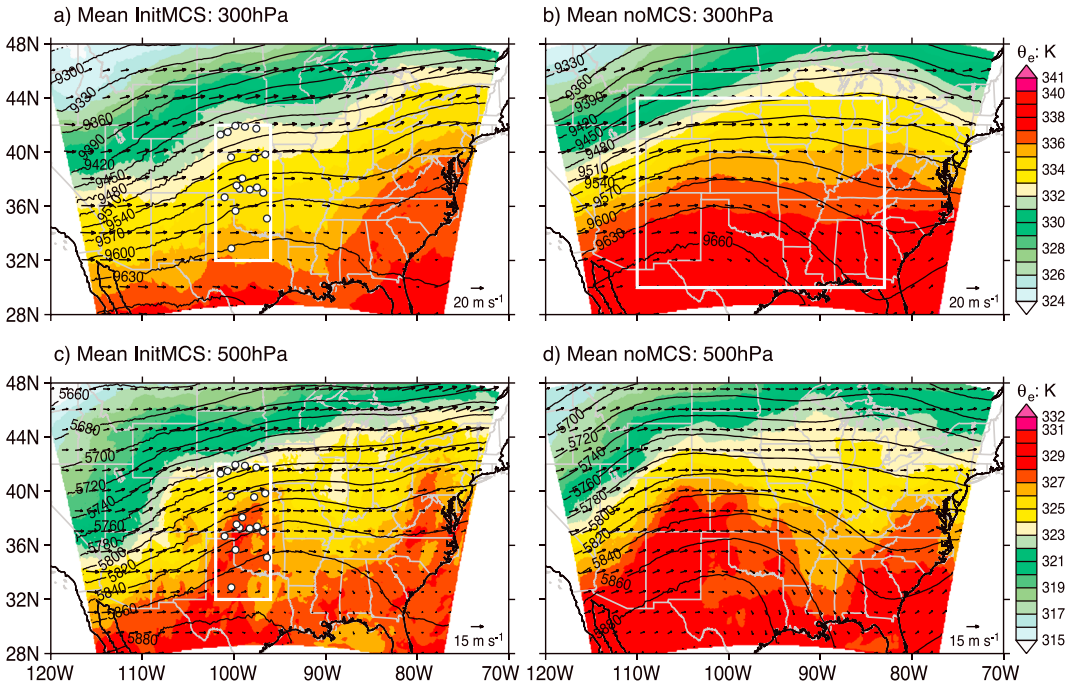

Figure 5. Composites of mean geopotential height (in meters, contour lines), wind (vector), and equivalent potential temperature (in K, color filled) at (a, b) 300 hPa and (c, d) 500 hPa for conditions with no MCS occurrences (Figures 5b and 5d) and at 0–3 h before MCS initiation (Figures 5a and 5c). The dots indicate the locations of MCS initiation. The box in Figures 5a and 5c is the region in which MCS initiation (initMCS) was identified. The box in Figure 5b is the region in which cases of no MCS initiation (noMCS) were identified. See section 2 for further information on the identification of times and locations of initiation and non-initiation.

4. Analysis Results

4.1. Environmental Conditions When MCSs Do and Do Not Initiate

It is generally thought by forecasters that MCSs are favored under certain synoptic conditions and disfavored in others. We tested that idea by using fixed-location composites for conditions corresponding to MCS or no MCS convection initiation over the Southern Great Plains to determine the characteristics of the synoptic environment at times of MCS initiation. Figure 5 shows the conditions at 300 and 500 hPa. Conventional thinking (as can be seen on many weather forecasting websites and documented by Maddox, 1983) is that conditions most favorable to convection are generally found ahead of a trough. Upward air motion concentrated in the region of southwest flow ahead of a northern hemispheric trough raises the relative humidity and destabilizes the air mass. The locations of initiation of the MCSs examined in this section were clustered over the Oklahoma-Kansas-Nebraska corridor in a southwesterly flow regime between a trough to the west and a ridge immediately to the east of the initiation zone (Figures 5a and 5c). Thus, the fixed-location composites confirm that MCSs formed in the region of southwest flow ahead of an upper-level trough. Furthermore, when no initiation occurred, the 300–500 hPa flow was more nearly westerly, with ridge conditions prevailing over the Oklahoma-Kansas-Nebraska region; trough conditions were located farther to the west than in the initiation cases.

Figure 6 shows the same patterns occurring at 700 hPa but more strongly than at 300 and 500 hPa. The region of strongest southwesterly winds was located in the center of the region of initiation and coincides with a maximum of equivalent potential temperature (θ_e) (Figure 6a). When there was no initiation, ridge conditions dominated, and the winds were lighter and more westerly, and θ_e values were lower (Figure 6b). Also shown in Figure 6 are the anomalies of wind, geopotential height, and θ_e. Figure 6c shows that the flow anomaly in the initiation zone was strongly southerly, so that moist air (with high θ_e) was being advected from the region of the Gulf of Mexico more than usual, which is another synoptic-scale factor consistent with MCSs flourishing in this region. In contrast, the anomaly flow in the cases of no initiation was nearly zero and actually weakly northerly along the eastern edge of the Oklahoma-Kansas-Nebraska corridor. Similar conditions prevailed at 850 hPa, with extremely strong southerly, high-θ_e flow into and through the initiation

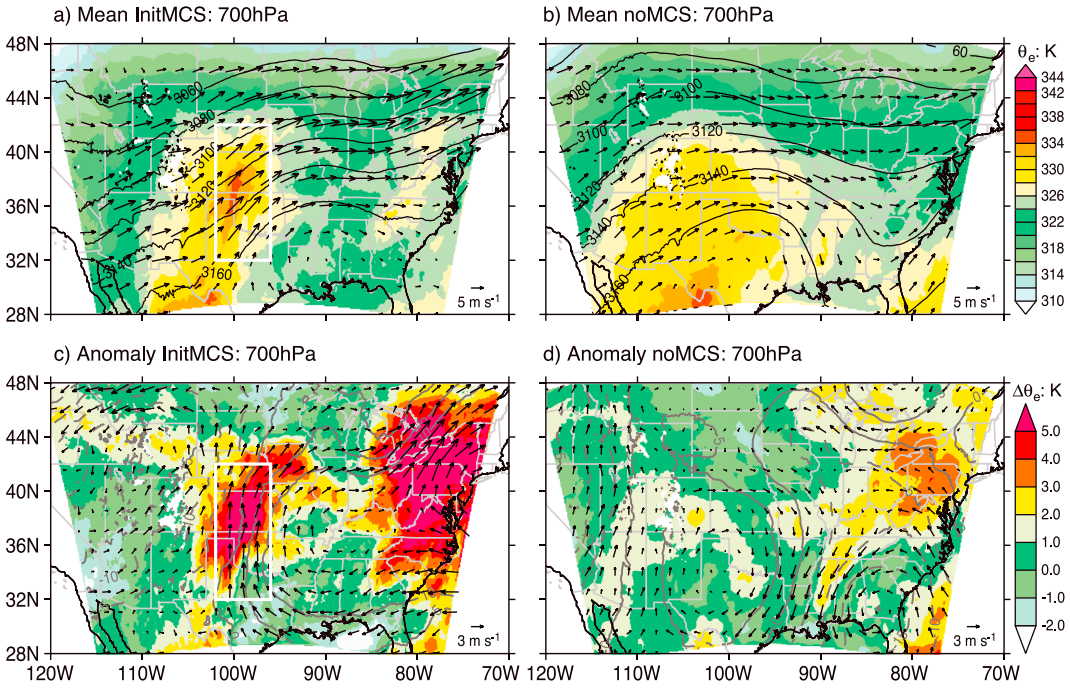

Figure 6. Composites of (a and b) mean and (c and d) anomaly geopotential height (in meters, contour lines), wind (vector), and equivalent potential temperature (in K, color filled) at 700 hPa for conditions with no-MCS occurrences (Figures 6b and 6d), and at 0–3 h before MCSs initiation (Figures 6a and 6c). Boxes and notation are the same as in Figure 5. Anomalies are calculated as deviation from the time mean for each hour of the day and for each month at each grid box to remove the mean seasonal and diurnal variations.

region (Figure 7a). The 850 hPa anomaly flow shown in Figure 7c is southerly with maximum strength in the center of the initiation zone, over Oklahoma and Kansas. The anomaly flow consisted of a confluence of southeasterly high-θ_e flow from the Gulf of Mexico and southwesterly drier flow from the Mexican Plateau, implying a tendency for dry lines (Bluestein, 1993, pp. 282–290) to be present in the initiation zone.

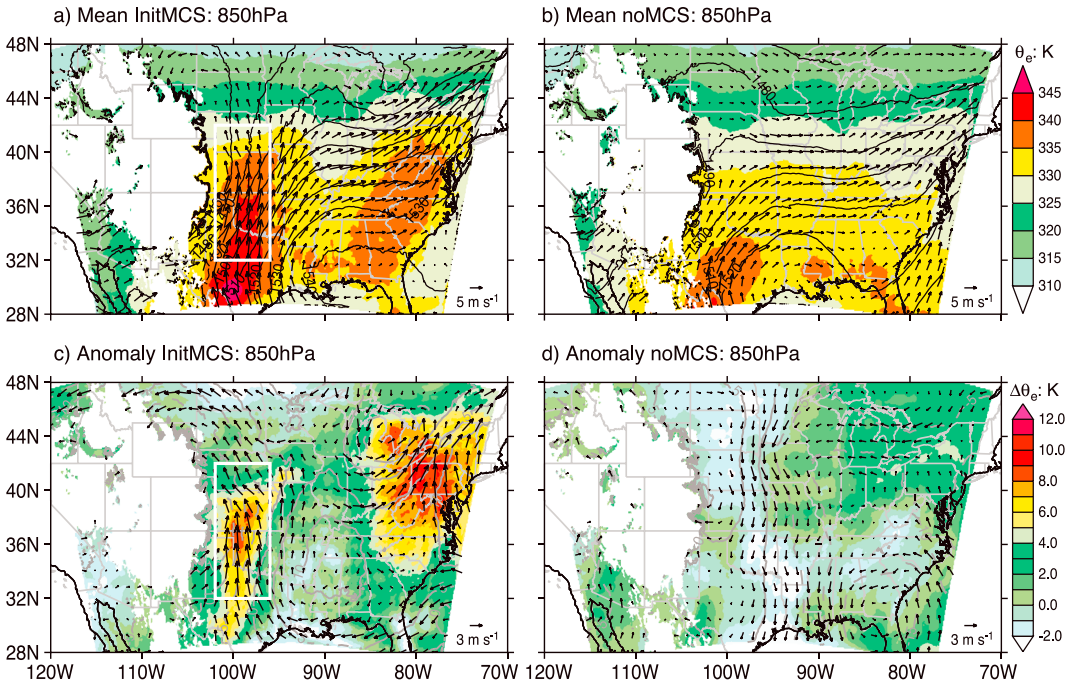

Figure 7. Similar to Figure 6 but for 850 hPa.

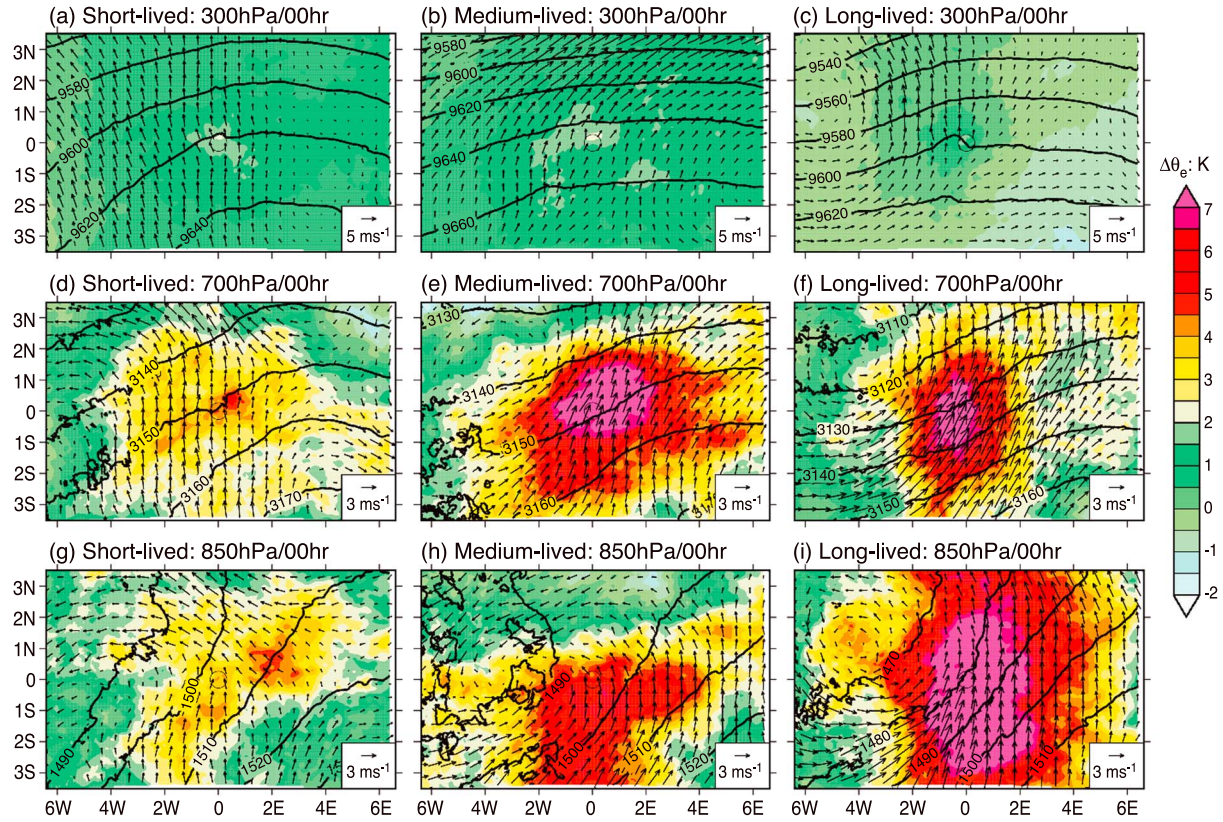

Figure 8. Relative-location composites of mean geopotential height (in meters, contour lines), anomaly wind (vector), and anomaly equivalent potential temperature ($\Delta\theta_e$, color filled) at 300 (Figures 8a–8c), 700 (Figures 8d–8f), and 850 hPa (Figures 8g–8i) at MCS initiation (00 h) for (a, d, and g) short-lived, (b, e, and h) medium-lived, and (c, f, and i) long-lived MCSs. The *x* and *y* axes show relative distances away from the composite centers (MCS geometric centers).

However, the bulk of the 850 hPa anomaly flow was from the Gulf and moist. The model composites in Figures 5–7 thus demonstrate objectively that the large-scale conditions were consistently favorable for MCS development in the initiation cases, while the anomaly flow in the cases of no MCS initiation was northerly, from dry regions, and therefore working against MCS development. These results are entirely of the expected nature based on Maddox (1983), conventional forecasting practice, and many other papers.

4.2. MCS Relative-Location Composite

Having established that large-scale environmental conditions were of an overall favorable character for MCS development in the initiation cases and not so in the noninitiation cases, we now use the relative-location composites of MCSs to examine features of the environment directly related to MCSs growing to different sizes. Specifically, we contrast composites of the model output for short-, medium-, and long-lived MCSs at the time of MCS initiation and at +6 h and +9 h after MCS initiation.

4.2.1. MCS Initiation Environment

The relative-location composites of wind, geopotential, and equivalent potential temperature do not show systematic differences among the short-, medium-, and long-lived systems 6 h before MCS initiation (not shown). However, by 3 h prior to and at the time of MCS initiation, the anomaly fields of wind and θ_e showed distinct differences between short-, medium-, and long-lived MCSs. Here we will examine the results at the time of initiation (referred to as 0 h), for each lifetime category. These results are similar to those 3 h prior to initiation (−3 h, not shown).

In the previous section, we saw that, in general, initiation was associated with a trough to the west. The geopotential height fields at all levels in Figure 8 show that the signature of the trough to the west (and ridge to the east) was most distinct for the long-lived MCSs. This signature is evident in the shape of height contours and their tighter gradient for the long-lived cases. The trough is also apparent for the medium- and short-lived MCSs but less distinctly so in shape and gradient of height contours. At the upper levels, a

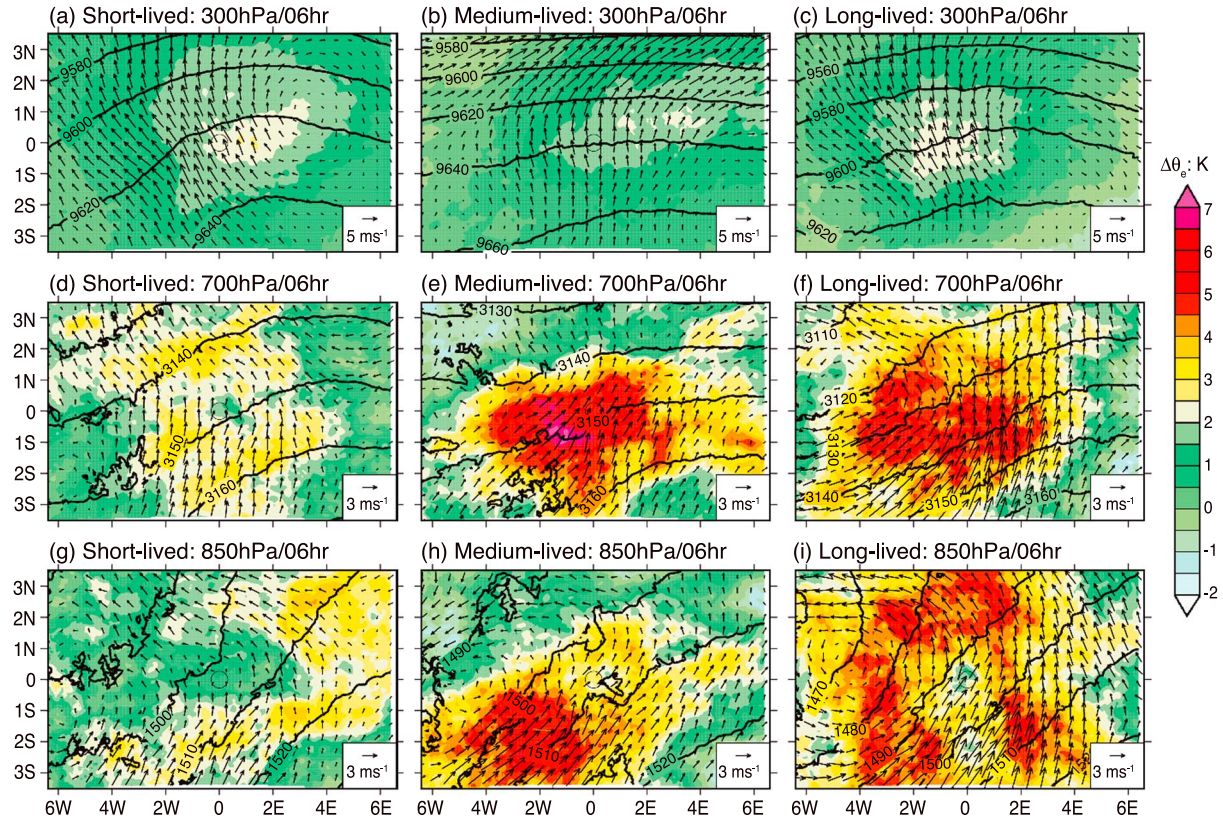

Figure 9. Similar to Figure 8 but at +06 h after MCS initiation.

difference in the jet at 300 hPa to the north of the composite center and the upper layer vertical wind shear is notable among the three categories of MCSs in that only the medium-lived MCSs show a strong upper-level jet and vertical wind shear, which are absent in the short- and long-lived MCSs.

The anomaly fields of wind and θ_e in Figure 8 further show that the longer lived the MCS, the stronger and more northward penetrating was the southwesterly flow supporting the systems. The longest-lived systems also had the strongest and northernmost extending tongue of anomalously high-θ_e air. Thus, the northward flux of high-θ_e air (wind speed times the horizontal gradient of θ_e) was largest and extended farthest northward in the cases of long-lived MCS. We will see later that this high-θ_e flux northward also coincided with the maximum northward flux of moisture.

Figures 8e and 8f show that, compared to the long-lived MCS cases, the region of high θ_e at 700 hPa spreads over a broader area in the medium-lived cases. In contrast, Figures 8h and 8i show that at 850 hPa the θ_e values were generally much lower in the medium-lived cases. Thus, at the initiation hour, the large-scale anomaly flow in the lower troposphere was strengthening the potential instability (i.e., driving the vertical gradient of θ_e to larger negative values) more in the long-lived cases than in the medium-lived cases. As we will see, the 850 hPa flow was anomalously moist and also providing low-level moisture to the MCSs.

The intensities of cyclonic flow anomalies increased from short-lived to long-lived MCSs at both 850 (Figures 8g–8i) and 700 hPa (Figures 8d–8f), and at 300 hPa; cyclonic vortices are only seen in the anomaly flow for the long-lived systems (Figure 8c). At 700 hPa, the long-lived MCSs are accompanied by a unique anomalous flow from west of the composite domain, which brings in relatively colder air (Figure 8f), which is likely to help sustain the shortwave trough and contribute to the narrower and more concentrated region of enhanced θ_e.

The foregoing described differences in relative-location composites computed for the time of initiation of short-, medium-, and long-lived systems suggest that the sustainability or longevity of the MCSs is favored by the large-scale environmental conditions within which they develop.

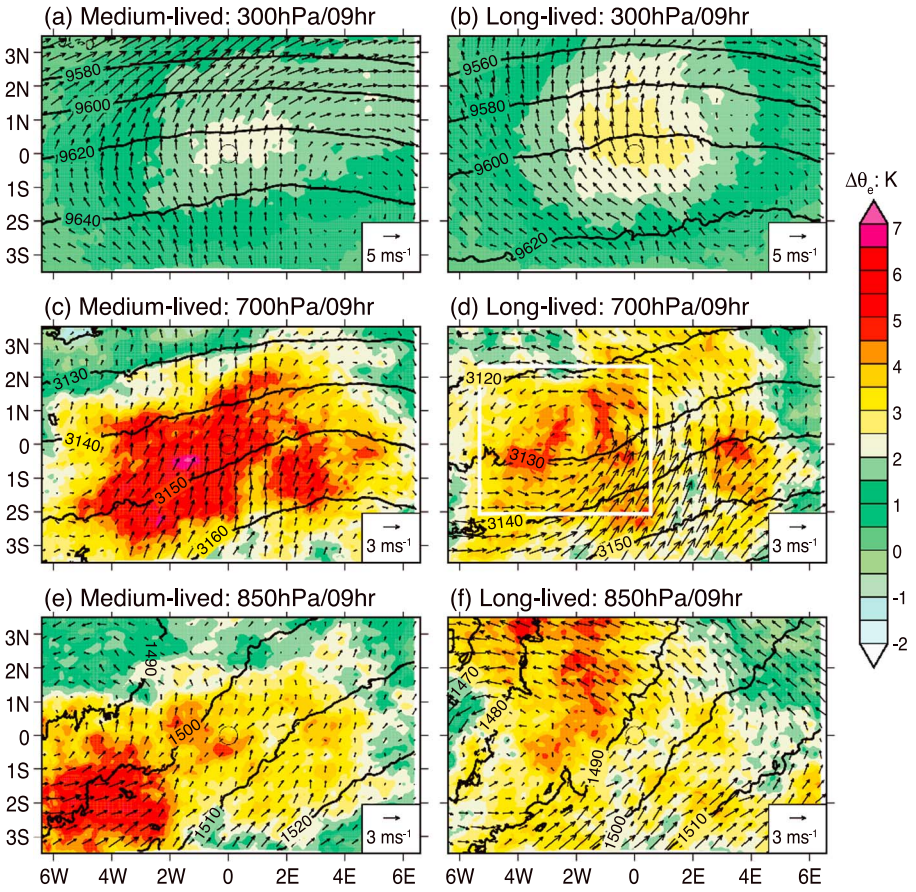

Figure 10. Similar to Figure 8 but at +09 h after MCS initiation. Box in Figure 10d shows region of heating profile calculation in Figure 11.

4.2.2. Environment 6 h After MCS Initiations

The relative-location composites for 6 h after the MCS initiation (+6 h) show the long-lived MCSs continuing to exhibit the most distinctive trough/ridge signature and strongest height gradients at each level (Figures 9c, 9f, and 9i). The most important new features at +6 h were in the anomaly wind field of the long-lived systems. At this time, mesoscale features were beginning to dominate the anomaly field. At 300 hPa a pronounced diffluent, divergent mesoscale signature emanates from the center of the long-lived MCS. At 700 and 850 hPa, a mesoscale vortex became more distinct ~5° on the west side of the center of the composite at both 850 and 700 hPa. This location would be in the trailing portion of an eastward moving MCS, where a stratiform precipitation region is expected. It is in that region, at these levels, where a mesoscale convective vortex (MCV) is expected in a robust MCS (Bartels & Maddox, 1991; Brandes, 1990; Chen & Frank, 1993; Davis & Weisman, 1994; Fritsch et al., 1994; Houze, 2004, 2014; Johnson & Bartels, 1992; Johnston, 1982; Leary & Rappaport, 1987; Raymond & Jiang, 1990; D. Zhang & Fritsch, 1987, 1988a, 1988b). Figures 9f and 9i show that the westerly component flow into the southwest side of the MCV was advecting low-θ_e air into the rear of the MCV. As such air is ingested into the rear of an MCS, it is ingested into the rear-to-front sloping mesoscale downdraft that contributes to the cold pool propagation of the MCS (Houze et al., 1989).

Figure 9 further shows a broader region of high-θ_e air at the 850 and 700 hPa levels in the long-lived systems than in the medium-lived systems, although the maximum θ_e values were somewhat smaller compared to the medium-lived systems. The lower values of θ_e may have been induced by the westerlies on the south side of the cyclonic center advecting cooler and drier air into the region at 700 hPa between 0 h (Figure 8f) and +6 h (Figure 9f). Comparison of the medium- and long-lived systems suggests that a stronger upper-level ridge and lower-level cyclone had been produced by convective heating. In a longer-lived MCS, this heating applied over the lifetime of the system likely created a quasi-balanced circulation,

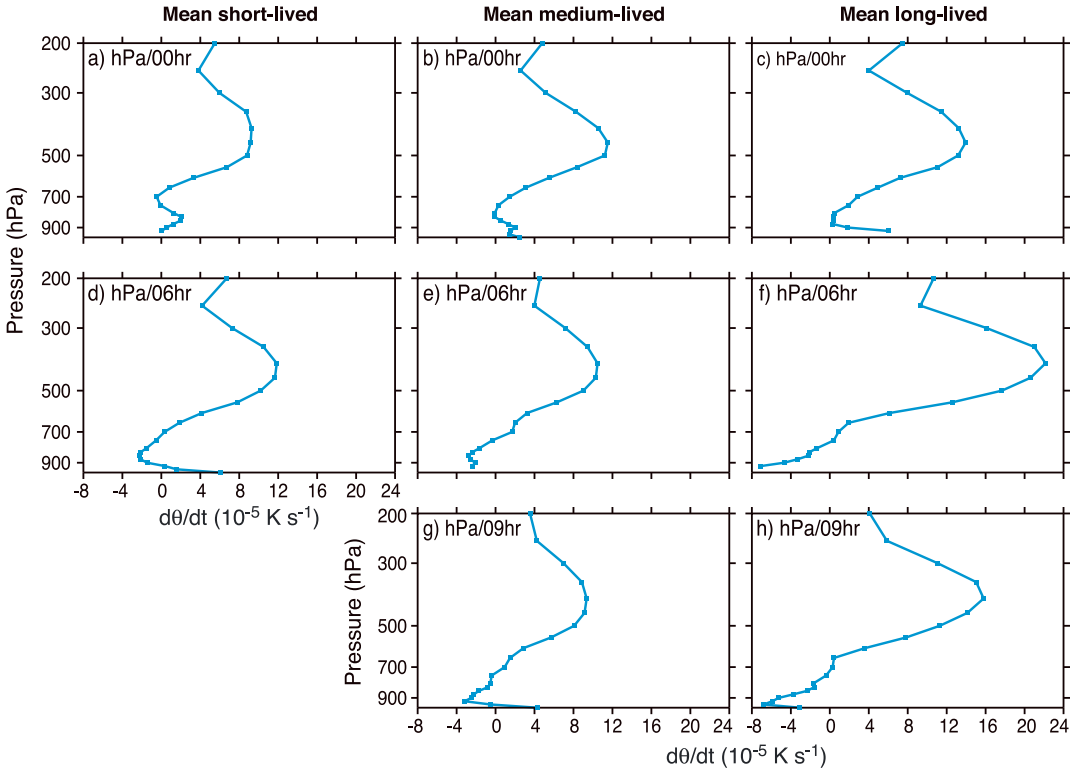

Figure 11. Vertical profiles of heating ($d\theta/dt$) averaged over the region shown in Figure 10d for the (a, d)short-lived, (b, e, and g) medium-lived, and (c, f, and h) long-lived MCSs at 00, +06, and +09 h after initiation.

which sustained the system by acting as a "dynamical flywheel" to support persistent deep vertical motion (Houze, 2014, pp. 284–286).

For the medium and short-lived systems at +6 h, the cyclonic anomaly flow feature was not distinctive at 700 hPa, but at 850 hPa, the medium-lived systems had an oval-shaped cyclonic flow anomaly centered slightly farther to the south than in the long-lived systems. This 700–850 hPa cyclonic flow anomaly of the medium-lived systems produced strong advection of high-θ_e air toward the system center. This pattern differs from that of the long-lived MCSs, which had due westerly flow advecting low-θ_e air into the rear of the MCS in the long-lived systems. The low-θ_e air injected into the west side of the MCS, where it would help to drive the mesoscale downdraft circulation in the trailing stratiform portion of the MCS and thus contribute to the longevity of the MCS.

4.2.3. Environment 9 h After MCS Initiations

The short-lived MCSs had dissipated by +9 h and are therefore not represented in Figure 10. Both the medium- and long-lived MCSs continued to show distinctive patterns in circulation and thermodynamics, especially at 700 hPa and above. The anomaly winds were stronger and more organized in the long-lived MCSs than in the medium-lived systems at both 850 and 700 hPa (Figures 10c–10f). Comparison of Figures 9f and 10d shows that the vortex at 700 hPa intensified from +6 h to +9 h in the long-lived systems, consistent with stratiform heating aloft and the cooling from evaporation and melting from below. This "top-heavy" heating profile generates potential vorticity at the midlevels (Fritsch et al., 1994; Houze, 2014, pp. 284–286). The generation of potential vorticity is the result of a heating profile that increases sharply with height. The heating profile in the relative-location composite shows that the vertical gradient of heating is most extreme at +6 and +9 h in the long-lived MCSs (Figure 11).

Figure 12 shows the precipitation composite for the short-, medium-, and long-lived MCSs at 0, 6, and 9 h. The MCSs produced significant precipitation at the center of the composite, but a spatially extensive precipitation area is also notable to the west of the long-lived MCSs. The MCSs occurring in this region (especially long-lived ones) almost always propagate eastward, with trailing stratiform precipitation (e.g., Houze et al. 1990). Therefore, the precipitation to the west in the composite was mostly likely stratiform. The mesoscale

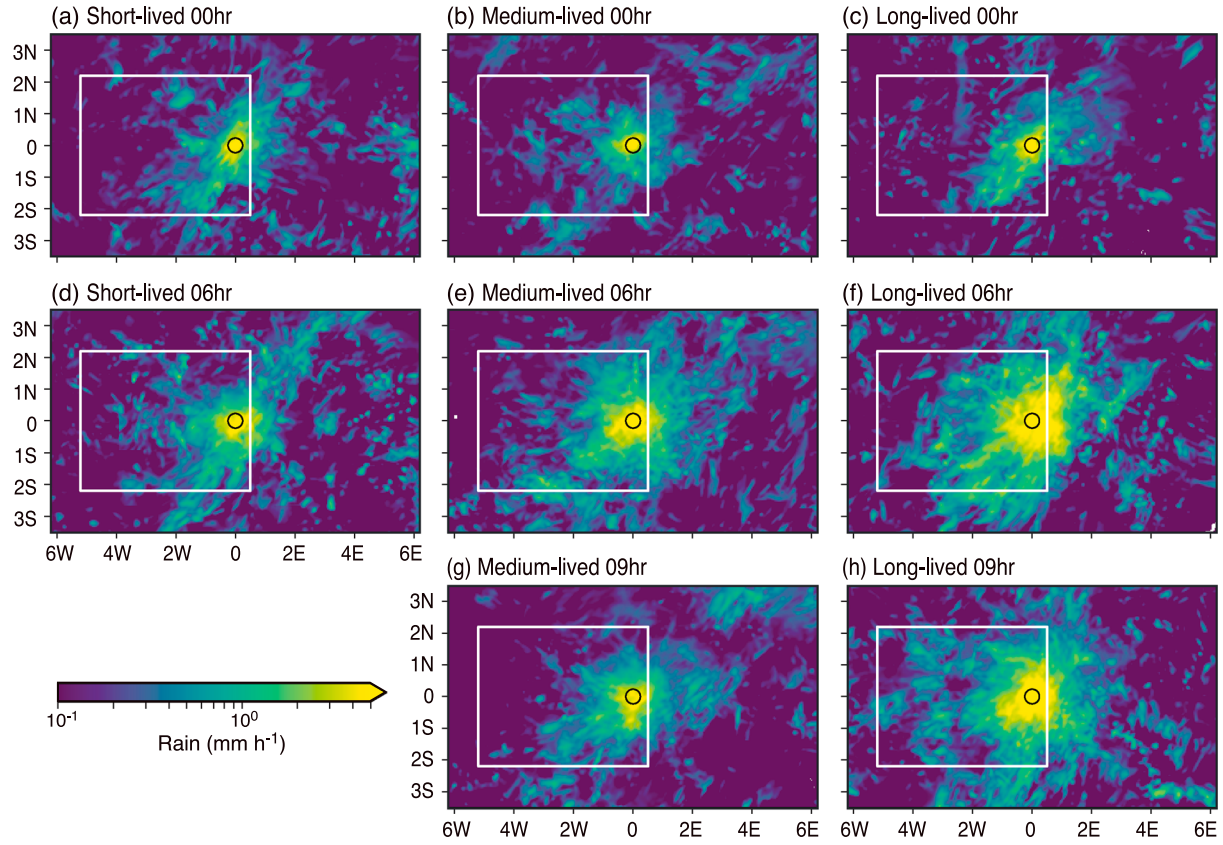

Figure 12. Relative-location composites of accumulated precipitation (mm h^{-1}) for the (a, d) short-lived, (b, e, and g) medium-lived, and (c, f, and h) long-lived MCSs at 00, +06, and +09 h after initiation. The white boundary denotes the same rectangular box shown in Figure 10d for calculation of the heating profiles shown in Figure 11.

vortex center seen in the composite wind anomaly field of Figure 9f is located west of the composite precipitation. Such a displacement is consistent with the fact that the MCSs forming the composite are generally of the form of eastward propagating squall lines with a leading line and trailing stratiform region. In this type of storm there is strong front-to-rear advection at upper levels within the MCS. The response to the stratiform precipitation would therefore be expected downstream of the precipitation. This precipitation composite thus shows spatial consistency between the heating profile, the trailing precipitation, and the vortex in the wind anomaly field for the long-lived MCSs. Although an MCV signature is suggested by both the medium- and long-lived MCS environment even at 0 h (Figures 8e and 8f), we find that it is only the mesoscale vortex of the anomaly wind field of the long-lived MCSs that notably strengthens and shifts toward the composite center over time. Such strengthening and shifting are consistent with the increasing contrast of the upper-level heating and lower-level cooling of the heating profile (Figure 11) that generates PV in the western sector of the composite long-lived MCSs (Figure 12). The MCV of the medium-lived MCSs is almost identical between 0 and 6 h (Figures 8e and 9e), in line with the nearly constant heating profile during that time period (Figures 11b and 11e). Hence, we attribute the growing difference of the MCV and MCS strength between the medium- and long-lived MCSs to the feedback from the MCSs to the circulation through diabatic heating that strengthens and sustains the long-lived MCSs relative to the medium-lived MCSs. It cannot be completely ruled out that the vortex pattern seen in the composite is due to strengthening of the synoptic-scale trough, which in turn drives a stronger mesoscale system with more rain. However, the association of the stronger vortex with the more top-heavy heating profile is circumstantially indicative of the presence of the feedback expected from a strong MCS.

Figure 10b further shows that at +9 h a clear MCS signature had developed at 300 hPa, where a patch of anomalously high-θ_e air had formed over the center of the MCS. This patch of high θ_e was located within the divergent wind anomaly. Both the divergence and high-θ_e anomalies are expected in a well-formed

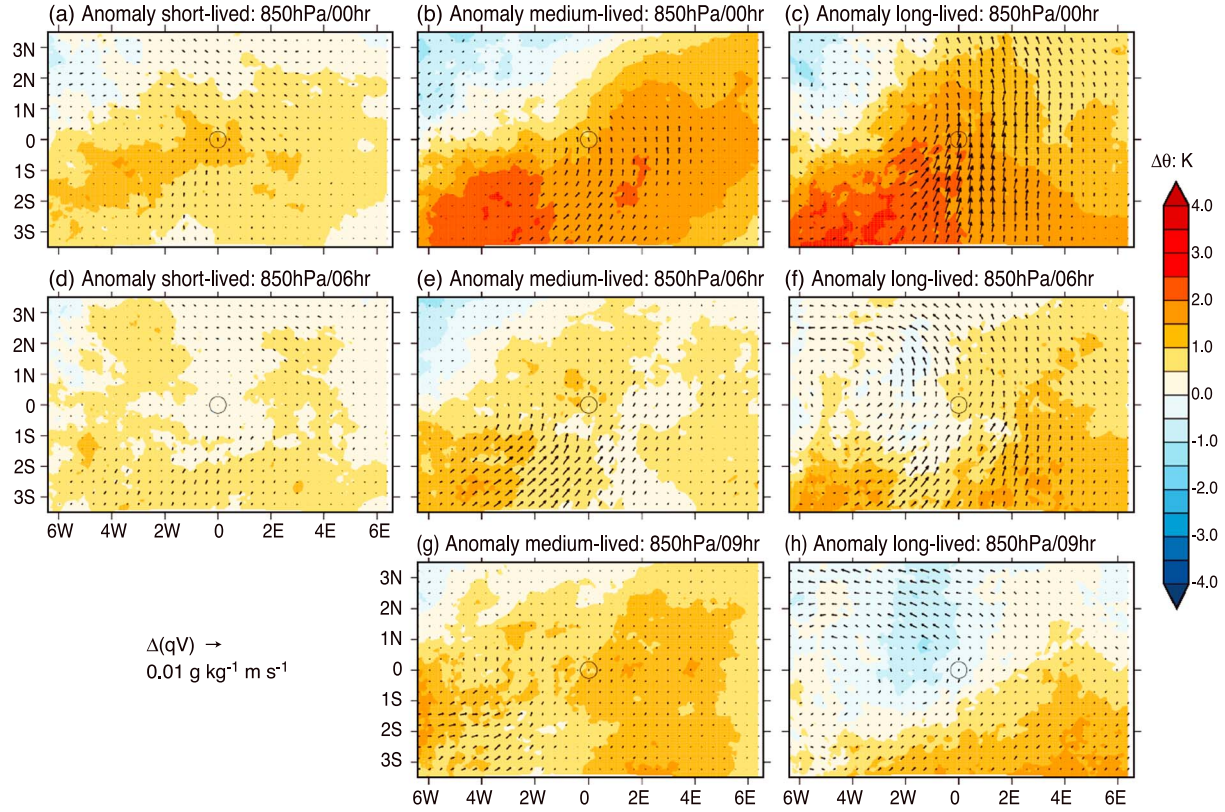

Figure 13. Relative-location composites of anomaly moisture flux and anomaly potential temperature ($\Delta\theta$, color filled) at 850 hPa at 00, +06, and +09 h after MCS initiation for (a, d) short-lived, (b, e, and g) medium-lived, and (c, f, and h) long-lived MCSs. The *x* and *y* axes show relative distances away from the composite centers (MCS geometric centers). The moisture flux is computed as water vapor mixing ratio (q) multiplying the corresponding horizontal wind vector ($\boldsymbol{V}$).

MCS. As seen in conceptual models (Houze, 2014, Chapters 6 and 9, pp. 156, 247; Houze et al., 1989; Yuter & Houze, 1995), the upper levels of an MCS become filled with high-θ_e air flowing out of the tops of the actively convective zones and being incorporated aloft in the divergent stratiform cloud regions.

The robust structure of the long-lived MCSs at +9 h is further seen in the 850 hPa moisture flux and potential temperature (θ) anomalies (Figure 13). Compared to the short- and medium-lived MCSs, the moisture flux into the center of the long-lived systems was stronger at 00 and 06 h, likely facilitating their longer lifetime and more distinct structure. By 09 h the moisture fluxes were declining. In addition, the θ patterns show the development of a strong 850 hPa cold core in the long-lived MCSs, which must be a result of the persistent melting and evaporational cooling that characterizes the broad stratiform precipitation regions of strong MCS (Houze, 2004; Houze, 2014, Chapter 9).

5. Conclusions

Regional simulations over the central United States during the boreal warm seasons (May–August) of 2011 and 2012 produce a population of MCSs that had characteristics similar to MCSs observed by radar and seen in infrared satellite imagery. Averages of meteorological variable fields (geographically fixed composites) when MCSs were initiating differed from those when no MCSs occurred. The no-initiation environment was dominated by a relatively strong ridge and an anticyclonic flow anomaly over the Great Plains, whereas MCSs initiated in the region of southwesterly flow ahead of a trough, as is well known from Maddox (1983), as well as other studies and general experience. In addition, when MCSs were forming over the Oklahoma-Kansas-Nebraska corridor, the climatological warm moist low-level south-southeasterly jet entering the region from the Gulf of Mexico was stronger and more laden with high-θ_e air than normal.

To examine the large-scale conditions in which the MCSs were embedded after initiation, we constructed averages of the model variables centered on each simulated MCS at 3, 6, and 9 h after their time of

formation (relative-location composites). Consistent with Coniglio et al. (2010), our simulations show a stronger and broader southerly LLJ that provides more moisture to sustain convection in the long-lived MCSs compared to the short- and medium-lived MCSs. Coniglio et al. (2010) noted that long-lived MCSs are associated with stronger deep-layer vertical wind shear compared to short-lived MCSs and that the shear is important for maintaining convection that feeds on the elevated unstable air after dark (Trier et al., 2006). By separately looking at short-, medium-, and long-lived MCSs, we find that only the medium-lived MCSs are associated with stronger upper layer vertical wind shear (Figures 8 and 9). This result suggests that there might be an optimal environmental shear for extra long life, with too much shear limiting the lifetime. Downward transport of momentum could lead to leading lines outrunning the trailing stratiform components of systems in the case of stronger shear. While such speculation seems reasonable, the role of vertical wind shear in the rapid development, maintenance, and dissipation of MCSs deserves future investigation. MCSs are expected to have their greatest impact on the large-scale flow when they are long-lived because mesoscale systems tend to generate a quasi-balanced circulation in midlevels as a result of the top-heavy diabatic heating profile associated with the stratiform regions common to long-lived MCSs (Fritsch et al., 1994; Houze, 2014, Chapter 9). The heating profile in the relative-location composites was most top heavy at the 9 h life stage. The environmental wind fields were also most strongly altered at 9 h, with a cyclonic anomaly centered in the western (likely stratiform) portion of the composite field at midlevels, while the upper levels had a strongly divergent anomaly field. Both features would be expected from the top-heavy heating occurring over several hours. Thus, the trough was strengthened by long-lived systems, making the midlevel large-scale trough conditions even more favorable for MCSs.

At 9 h, the cyclonic circulation anomaly was advecting low-θ_e air into the MCS region from the west, thus providing air favorable to support evaporatively driven mesoscale downdrafts in the stratiform regions of MCSs. The more robust (longer-lived and larger) stratiform regions enhance the top-heavy heating profile and thus strengthen the mesoscale circulation of the MCS, which provides the MCS with the flywheel effect (Houze, 2014, pp. 284–286) that promotes the longer duration of the MCS. In addition, in the geographical region of this study, the mesoscale anomaly circulation of the long-lived MCSs supported their long durations by means of a strengthened southerly component low-level jet from the Gulf of Mexico, which brought increased amounts of high-θ_e air into the MCSs and fed the active convective updrafts on the southern and eastern edges of the MCSs.

Most of the above described features were present in the model output to a lesser degree for MCSs lasting 9 h but much less perceptible for MCSs lasting only 6 h. These results call attention to the importance of recognizing long-lived MCSs in simulations aimed at understanding changes in the large-scale circulation and climate. Long-lived MCSs have long been recognized by weather forecasters not only as producers of large amounts of precipitation, severe storms, and floods but also as agents of change that affect the short-term forecasting of the synoptic-scale circulation (e.g., Stensrud, 1996). Our simulations conducted over entire seasons at convection-permitting resolution capture the repeated occurrence of MCSs over the central United States and show that when MCSs are long lived they occur in certain recognizable synoptic conditions, in association with an enhanced low-level jet from the Gulf of Mexico and located ahead of a strong synoptic-scale trough, which is, already stronger than in the synoptic conditions of short- and medium-lived MCSs during initiation. In addition, the seasonal simulations show that the long-lived MCSs alter those synoptic conditions in ways that constitute a positive feedback to the synoptic-scale flow. Future work should investigate the relative role of the synoptic conditions during initiation versus the positive feedback from the MCSs on the synoptic conditions in maintaining long-lived MCSs.

Overall, our analyses highlight three major challenges for simulating MCSs in climate models related to how well they capture the distinct large-scale environments favorable for MCS development, their representation of convection and its organization, and their ability to simulate the upscale feedbacks of MCSs on the mesoscale and large-scale circulations associated with the diabatic heating in the stratiform regions. Due to the positive feedback from MCSs to the circulation, it follows that even small changes in the large-scale environment may amplify the change in longevity of MCSs in a warmer climate. Changes in the longevity of MCSs can subsequently influence the heavy rainfall produced by MCSs, as evident from Feng et al. (2016) that attributed the observed increase in total and extreme precipitation in the central United States to an increased frequency of longer-lived MCSs. As the positive feedback by MCSs on large-scale circulation is most

evident in long-lived MCSs, modeling the latter and its interactions with the large-scale environment is critical for understanding regional and global water cycle changes in the future. Knowledge of the statistical behaviors of MCSs elucidated in this study using convection-permitting simulations will be useful in the development of methods to represent the occurrence and effects of MCSs in lower-resolution models used to evaluate changes in the global circulation, water cycle, and climate over longer time periods.

Acknowledgments

This study is supported by the U.S. Department of Energy Office of Science Biological and Environmental Research (BER) as part of the Regional and Global Climate Modeling program. Professor Houze's University of Washington participation is supported by the Pacific Northwest National Laboratory under Task Order 292896 (WACCEM) of Master Agreement 243766. We want to thank three anonymous reviewers for their careful and constructive comments that have helped us improve our manuscript. The authors also thank Casey Burleyson for processing the satellite infrared data set and Xiquan Dong for providing access to the NMQ radar data set. This research used computational resources from the National Energy Research Scientific Computing Center (NERSC), a DOE User Facility supported by the Office of Science under contract DE-AC02-05CH11231. PNNL is operated for DOE by Battelle Memorial Institute under contract DE-AC05-76RL01830. Sounding data were obtained from the Atmospheric Radiation Measurement (ARM) Climate Research Facility, a U.S. Department of Energy Office of Science user facility sponsored by the Office of Biological and Environmental Research. The global satellite infrared data set was obtained from NASA Goddard Earth Sciences Data and Information Services Center when conducting this work. The data set is now hosted at the NOAA Climate Prediction Center (http://www.cpc.ncep.noaa.gov/products/global_precip/html/wpage.full_res.shtml). All data and simulation output used in this study are archived at NERSC and can be accessed by contacting L. Ruby Leung (ruby.leung@pnnl.gov).

References

Barnes, H. C., Zuluaga, M. D., & Houze, R. A. (2015). Latent heating characteristics of the MJO computed from TRMM observations. *Journal of Geophysical Research: Atmospheres*, *120*, 1322–1334. https://doi.org/10.1002/2014JD022530

Bartels, D. L., & Maddox, R. A. (1991). Midlevel cyclonic vortices generated by mesoseale convective systems. *Monthly Weather Review*, *119*(1), 104–118. https://doi.org/10.1175/1520-0493(1991)119%3C0104:mcvgbm%3E2.0.co;2

Bluestein, H. B. (1993). *Synoptic dynamic meteorology in midlatitudes, vol. II, observations and theory of weather systems* (594 pp.). New York: Oxford University Press.

Brandes, E. A. (1990). Evolution and structure of the 6–7 May 1985 mesoscale convective system and associated vortex. *Monthly Weather Review*, *118*(1), 109–127. https://doi.org/10.1175/1520-0493(1990)118%3C0109:easotm%3E2.0.co;2

Carbone, R. E., Tuttle, J. D., Ahijevych, D. A., & Trier, S. B. (2002). Inferences of predictability associated with warm season precipitation episodes. *Journal of the Atmospheric Sciences*, *59*(13), 2033–2056. https://doi.org/10.1175/1520-0469(2002)059%3C2033:lopaww%3E2.0.Co;2

Chen, S. S., & Frank, W. M. (1993). A numerical study of the genesis of extratropical convective mesovortices. Part I: Evolution and dynamics. *Journal of the Atmospheric Sciences*, *50*(15), 2401–2426. https://doi.org/10.1175/1520-0469(1993)050%3C2401:ansotg%3E2.0.co;2

Cheng, C.-P., & Houze, R. A. Jr. (1979). The distribution of convective and mesoscale precipitation in GATE radar echo patterns. *Monthly Weather Review*, *107*(10), 1370–1381. https://doi.org/10.1175/1520-0493(1979)107%3C1370:tdocam%3E2.0.co;2

Chong, M., & Hauser, D. (1989). A tropical squall line observed during the COPT 81 experiment in west Africa. Part II: Water budget. *Monthly Weather Review*, *117*(4), 728–744. https://doi.org/10.1175/1520-0493(1989)117%3C0728:atslod%3E2.0.co;2

Chou, M.-D., & Suarez, M. J. (1994). An efficient thermal infrared radiation parameterization for use in general circulation models (Vol. 10, 85 pp.). NASA/TM-104606.

Coniglio, M. C., Hwang, J. Y., & Stensrud, D. J. (2010). Environmental factors in the upscale growth and longevity of MCSs derived from rapid update cycle analyses. *Monthly Weather Review*, *138*, 3514–3539. https://doi.org/10.1175/2010MWR3233.1; Corrigendum, 139, 2686–2688, doi:10.1175/MWR-D-11-00064.1

Cotton, W. R., Bryan, G., & van den Heever, S. (2011). *Storm and cloud dynamics* (2nd ed., 820 pp.). London, UK: Academic Press.

Cotton, W. R., Lin, M.-S., McAnelly, R. L., & Tremback, C. J. (1989). As composite model of mesoscale convective complexes. *Monthly Weather Review*, *117*, 765–783.

Coulter, R., Prell, J., Ritsche, M., & Holdridge, D. (1994). updated daily. Balloon-borne sounding system (SONDEWNPN). Oct 2010–March 2011, 36° 36′ 18.0″ N, 97° 29′ 6.0″ W: Southern Great Plains Central Facility (C1). Atmospheric Radiation Measurement (ARM) Climate Research Facility Data Archive: Oak Ridge, Tennessee, USA. Data set accessed 2015–01-01 at https://doi.org/10.5439/1021460

Davis, C. A., Ahijevych, A., & Trier, S. B. (2002). Detection and prediction of warm season midtropospheric vortices by the rapid update cycle. *Monthly Weather Review*, *130*, 24–42.

Davis, C. A., & Weisman, M. L. (1994). Balanced dynamics of mesoscale vortices produced in simulated convective systems. *Journal of the Atmospheric Sciences*, *51*(14), 2005–2030. https://doi.org/10.1175/1520-0469(1994)051%3C2005:bdomvp%3E2.0.co;2

Diffenbaugh, N. S., Scherer, M., & Trapp, R. J. (2013). Robust increases in severe thunderstorm environments in response to greenhouse forcing. *Proceedings of the National Academy of Sciences of the United States of America*, *110*(41), 16,361–16,366. https://doi.org/10.1073/pnas.1307758110

Doswell, C. A. III, Brooks, H. E., & Maddox, R. A. (1996). Flash flood forecasting: An ingredients-based methodology. *Weather Forecasting*, *11*, 560–581.

Feng, Z., Dong, X., Xi, B., McFarlane, S. A., Kennedy, A., Lin, B., & Minnis, P. (2012). Life cycle of midlatitude deep convective systems in a Lagrangian framework. *Journal of Geophysical Research*, *117*, D23201. https://doi.org/10.1029/2012JD018362

Feng, Z., Leung, L. R., Hagos, S., Houze, R. A., Burleyson, C. D., & Balaguru, K. (2016). More frequent intense and long-lived storms dominate the springtime trend in central US rainfall. *Nature Communications*, *7*, 13429. https://doi.org/10.1038/ncomms13429

Frank, N. L. (1970). Atlantic tropical systems of 1969. *Monthly Weather Review*, *98*(4), 307–314. https://doi.org/10.1175/1520-0493(1970)098%3C0307:atso%3E2.3.co;2

Fritsch, J. M., & Forbes, G. S. (2001). Mesoscale convective systems. *Meteorological Monographs*, *28*(50), 323–358. https://doi.org/10.1175/0065-9401-28.50.323

Fritsch, J. M., Kane, R. J., & Chelius, C. R. (1986). The contribution of mesoscale convective weather systems to the warm-season precipitation in the United States. *Journal of Climate and Applied Meteorology*, *25*(10), 1333–1345. https://doi.org/10.1175/1520-0450(1986)025%3C1333:TCOMCW%3E2.0.CO;2

Fritsch, J. M., Murphy, J. D., & Kain, J. S. (1994). Warm core vortex amplification over land. *Journal of the Atmospheric Sciences*, *51*(13), 1780–1807. https://doi.org/10.1175/1520-0469(1994)051%3C1780:wcvaol%3E2.0.co;2

Gamache, J. F., & Houze, R. A. Jr. (1982). Mesoscale air motions associated with a tropical squall line. *Monthly Weather Review*, *110*(2), 118–135. https://doi.org/10.1175/1520-0493(1982)110%3C0118:mamawa%3E2.0.co;2

Gamache, J. F., & Houze, R. A. Jr. (1985). Further analysis of the composite wind and thermodynamic structure of the 12 September GATE squall line. *Monthly Weather Review*, *113*(8), 1241–1260. https://doi.org/10.1175/1520-0493(1985)113%3C1241:faotcw%3E2.0.co;2

Gao, Y., Leung, L. R., Zhao, C., & Hagos, S. (2017). Sensitivity of U.S. summer precipitation to model resolution and convective parameterizations across gray zone resolutions. *Journal of Geophysical Research: Atmospheres*, *122*, 2714–2733. https://doi.org/10.1002/2016JD025896

Hagos, S., Feng, Z., McFarlane, S., & Leung, L. R. (2013). Environment and the lifetime of tropical deep convection in a cloud-permitting regional model simulation. *Journal of the Atmospheric Sciences*, *70*(8), 2409–2425. https://doi.org/10.1175/JAS-D-12-0260.1

Hamilton, R. A., Archbold, J. W., & Douglas, C. K. M. (1945). Meteorology of Nigeria and adjacent territory. *Quarterly Journal of the Royal Meteorological Society*, *71*(309–310), 231–264. https://doi.org/10.1002/qj.49707130905

Hartmann, D. L., Hendon, H. H., & Houze, R. A. (1984). Some implications of the mesoscale circulations in tropical cloud clusters for large-scale dynamics and climate. *Journal of the Atmospheric Sciences*, *41*(1), 113–121. https://doi.org/10.1175/1520-0469(1984)041%3C0113:SIOTMC%3E2.0.CO;2

Hong, S.-Y., Noh, Y., & Dudhia, J. (2006). A new vertical diffusion package with an explicit treatment of entrainment processes. *Monthly Weather Review*, *134*(9), 2318–2341. https://doi.org/10.1175/MWR3199.1

Houze, R. A. Jr., Smull, B. F., & Dodge, P. (1990). Mesoscale organization of springtime rainstorms in Oklahoma. *Monthly Weather Review*, *118*, 613–654.

Houze, R. A. (1977). Structure and dynamics of a tropical squall-line system. *Monthly Weather Review*, *105*, 1540–1567.

Houze, R. A. (1982). Cloud clusters and large-scale vertical motions in the tropics. *Journal of the Meteorological Society of Japan*, *60*(1), 396–410. https://doi.org/10.2151/jmsj1965.60.1_396

Houze, R. A. (1989). Observed structure of mesoscale convective systems and implications for large-scale heating. *Quarterly Journal of the Royal Meteorological Society*, *115*(487), 425–461. https://doi.org/10.1002/qj.49711548702

Houze, R. A. (2004). Mesoscale convective systems. *Reviews of Geophysics*, *42*, RG4003.

Houze, R. A. (2014). *Cloud dynamics* (2nd ed., 432 pp.). Oxford: Elsevier/Academic Press.

Houze, R. A.,& Betts, A. K. (1981). Convection in GATE. *Review of Geophysics and Space Physics*, *19*, 541–576.

Houze, R. A., Biggerstaff, M. I., Rutledge, S. A., & Smull, B. F. (1989). Interpretation of Doppler weather radar displays of midlatitude mesoscale convective systems. *Bulletin of the American Meteorological Society*, *70*(6), 608–619. https://doi.org/10.1175/1520-0477(1989)0702.0.CO;2

Janowiak, J. E., Joyce, R. J., & Yarsh, Y. (2001). A real-time global half-hourly pixel-resolution infrared dataset and its applications. *Bulletin of the American Meteorological Society*, *82*(2), 205–217. https://doi.org/10.1175/1520-0477(2001)082%3C0205:artghh%3E2.3.co;2

Jensen, M. P., Petersen, W. A., Bansemer, A., Bharadwaj, N., Carey, L. D., Cecil, D. J., … Zipser, E. J. (2016, 9). The midlatitude continental convective clouds experiment (MC3E). *Bulletin of the American Meteorological Society*, *97*, 1667–1686. https://doi.org/10.1175/Bams-D-14-00228.1

Johnson, R. H., & Bartels, D. L. (1992). Circulations associated with a mature-to-decaying midlatitude mesoscale convective system. Part II: Upper-level features. *Monthly Weather Review*, *120*(7), 1301–1321. https://doi.org/10.1175/1520-0493(1992)120%3C1301:cawamt%3E2.0.co;2

Johnston, E. C. (1982). Mesoscale vorticity centers induced by mesoscale convective complexes. Paper presented at 9th Conference on Weather Forecasting and Analysis, American Meteorological Society, Boston, Seattle, Washington.

Kane, R. J., Chelius, C. R., & Fritsch, J. M. (1987). Precipitation characteristics of mesoscale convective weather systems. *Journal of Climate and Applied Meteorology*, *26*(10), 1345–1357. https://doi.org/10.1175/1520-0450(1987)026%3C1345:Pcomcw%3E2.0.Co;2

Laing, A. G., & Fritsch, J. M. (2000). The large-scale environments of the global populations of mesoscale convective complexes. *Monthly Weather Review*, *128*, 2756–2776. https://doi.org/10.1175/1520-0493(2000)128%3C2756:TLSEOT%3E2.0.CO;2

Leary, C. A., & Houze, R. A. (1979). The structure and evolution of convection in a tropical cloud cluster. *Journal of the Atmospheric Sciences*, *36*(3), 437–457. https://doi.org/10.1175/1520-0469(1979)036%3C0437:tsaeoc%3E2.0.co;2

Leary, C. A., & Rappaport, E. N. (1987). The life-cycle and internal structure of a mesoscale convective complex. *Monthly Weather Review*, *115*(8), 1503–1527. https://doi.org/10.1175/1520-0493(1987)115%3C1503:Tlcais%3E2.0.Co;2

Li, Y., & Smith, R. B. (2010). The detection and significance of diurnal pressure and potential vorticity anomalies east of the Rockies. *Journal of Atmospheric Sciences*, *67*, 2734–2751. https://doi.org/10.1175/2010JAS3421.3

Liu, C., Ikeda, K., Rasmussen, R., Barlage, M., Newman, A. J., Prein, A. F., … Yates, D. (2016). Continental-scale convection-permitting modeling of the current and future climate of North America. *Climate Dynamics*. https://doi.org/10.1007/s00382-016-3327-9

Maddox, R. A. (1980). Meoscale convective complexes. *Bulletin of the American Meteorological Society*, *61*(11), 1374–1387. https://doi.org/10.1175/1520-0477(1980)0612.0.CO;2

Maddox, R. A. (1983). Large-scale meteorological conditions associated with midlatitude, mesoscale convective complexes. *Monthly Weather Review*, *111*(7), 1475–1493. https://doi.org/10.1175/1520-0493(1983)111%3C1475:LSMCAW%3E2.0.CO;2

Mapes, B., Tulich, S., Lin, J., & Zuidema, P. (2006). The mesoscale convection life cycle: Building block or prototype for large-scale tropical waves? *Dynamics of Atmospheres and Oceans*, *42*(1–4), 3–29. https://doi.org/10.1016/j.dynatmoce.2006.03.003

Markowski, P. M., & Richardson, Y. (2010). *Mesoscale meteorology in midlatitudes*, (p. 407). Chichester, UK: Wiley-Blackwell.

Martin, D. W., & Suomi, V. E. (1972). A satellite study of cloud clusters over the tropical North Atlantic Ocean. *Bulletin of the American Meteorological Society*, *53*, 135–156.

Mlawer, E. J., Taubman, S. J., Brown, P. D., Iacono, M. J., & Clough, S. A. (1997). Radiative transfer for inhomogeneous atmospheres: RRTM, a validated correlated-k model for the longwave. *Journal of Geophysical Research*, *102*, 16,663–16,682. https://doi.org/10.1029/97JD00237

Morrison, H., Thompson, G., & Tatarskii, V. (2009). Impact of cloud microphysics on the development of trailing stratiform precipitation in a simulated squall line: Comparison of one- and two-moment schemes. *Monthly Weather Review*, *137*(3), 991–1007. https://doi.org/10.1175/2008mwr2556.1

Nesbitt, S. W., Zipser, E. J., & Cecil, D. J. (2000). A census of precipitation features in the tropics using TRMM: Radar, ice scattering, and lightning observations. *Journal of Climate*, *13*(23), 4087–4106. https://doi.org/10.1175/1520-0442(2000)013%3C4087:acopfi%3E2.0.co;2

Payne, S. W., & McGarry, M. M. (1977). The relationship of satellite inferred convective activity to easterly waves over west Africa and the adjacent ocean during phase III of GATE. *Monthly Weather Review*, *105*, 413–420. https://doi.org/10.1175/1520-0493(1977)105<0413:TROSIC>2.0.CO;2

Peters, J. M., & Schumacher, R. S. (2014). Objective categorization of heavy-rain-producing MCS synoptic types by rotated principal component analysis. *Monthly Weather Review*, *142*(5), 1716–1737. https://doi.org/10.1175/MWR-D-13-00295.1

Pinto, J. O., Grim, J. A., & Steiner, M. (2015). Assessment of the high-resolution rapid refresh model's ability to predict mesoscale convective systems using object-based evaluation. *Weather Forecasting*, *30*, 892–913.

Pritchard, M. S., Moncrieff, M. W., & Somerville, R. C. (2011). Orogenic propagating precipitation systems over the United States in a global climate model with embedded explicit convection. *Journal of the Atmospheric Sciences*, *68*, 1821–1840.

Rasmussen, K. L., Hill, A. J., Toma, V. E., Zuluaga, M. D., Webster, P. J., & Houze, R. A. (2015). Multiscale analysis of three consecutive years of anomalous flooding in Pakistan. *Quarterly Journal of the Royal Meteorological Society*, *141*(689), 1259–1276. https://doi.org/10.1002/qj.2433

Raymond, D. J., & Jiang, H. (1990). A theory for long-lived mesoscale convective systems. *Journal of the Atmospheric Sciences*, *47*(24), 3077–3067. https://doi.org/10.1175/1520-0469(1990)047%3C3067:atfllm%3E2.0.co;2

Rotunno, R., Klemp, J. B., & Weisman, M. L. (1988). A theory for strong, long-lived squall lines. *Journal of the Atmospheric Sciences*, *45*(3), 463–485. https://doi.org/10.1175/1520-0469(1988)045%3C0463:atfsll%3E2.0.co;2

Rutledge, S. A., & Houze, R. A. Jr. (1987). A diagnostic modelling study of the trailing stratiform region of a midlatitude squall line. *Journal of the Atmospheric Sciences*, *44*(18), 2640–2656. https://doi.org/10.1175/1520-0469(1987)044%3C2640:admsot%3E2.0.co;2

Schumacher, C., Houze, R. A., & Kraucunas, I. (2004). The tropical dynamical response to latent heating estimates derived from the TRMM precipitation radar. *Journal of the Atmospheric Sciences*, *61*(12), 1341–1358. https://doi.org/10.1175/1520-0469(2004)061%3C1341:TTDRTL%3E2.0.CO;2

Skamarock, W. C., Klemp, J. B., Dudhia, J., Gill, D. O., Barker, D. M., Duda, M., … Powers, J. G. (2008). A description of the advanced research WRF version 3 (NCAR Technical Note).

Stensrud, D. J. (1996). Effects of persistent, midlatitude mesoscale regions of convection on the large-scale environment during the warm season. *Journal of the Atmospheric Sciences*, *53*(23), 3503–3527. https://doi.org/10.1175/1520-0469(1996)053%3C3503:eopmmr%3E2.0.co;2

Trapp, R. J., & Hoogewind, K. A. (2016). The realization of extreme tornadic storm events under future anthropogenic climate change. *Journal of Climate*, *29*(14), 5251–5265. https://doi.org/10.1175/Jcli-D-15-0623.1

Trier, S. B., Davis, C. A., Ahijevych, D. A., Weisman, M. L., & Bryan, G. H. (2006). Mechanisms supporting long-lived episodes of propagating nocturnal convection within a 7-day WRF model simulation. *Journal of the Atmospheric Sciences*, *63*, 2437–2461.

Weisman, M. L., Skamarock, W. C., & Klemp, J. B. (1997). The resolution dependence of explicitly modeled convective systems. *Monthly Weather Review*, *125*, 527–548.

Yang, G. Y., & Slingo, J. (2001). The diurnal cycle in the Tropics. *Monthly Weather Review*, *129*(4), 784–801. https://doi.org/10.1175/1520-0493(2001)129%3C0784:Tdcitt%3E2.0.Co;2

Yuan, J., & Houze, R. A. (2010). Global variability of mesoscale convective system anvil structure from A-Train Satellite Data. *Journal of Climate*, *23*(21), 5864–5888.

Yuter, S. E., & Houze, R. A. (1995). Three-dimensional kinematic and microphysical evolution of Florida cumulonimbus. Part II: Frequency distributions of vertical velocity, reflectivity, and differential reflectivity. *Monthly Weather Review*, *123*(7), 1941–1963. https://doi.org/10.1175/1520-0493(1995)123%3C1941:TDKAME%3E2.0.CO;2

Zhang, D.-L., & Fritsch, J. M. (1987). Numerical simulation of the meso-β scale structure and evolution of the 1977 Johnstown flood. Part II: Inertially stable warm-core vortex and the mesoscale convective complex. *Journal of the Atmospheric Sciences*, *44*(18), 2593–2612. https://doi.org/10.1175/1520-0469(1987)044%3C2593:nsotms%3E2.0.co;2

Zhang, D.-L., & Fritsch, J. M. (1988a). Numerical sensitivity experiments of varying model physics on the structure, evolution and dynamics of two mesoscale convective systems. *Journal of the Atmospheric Sciences*, *45*(2), 261–293. https://doi.org/10.1175/1520-0469(1988)045%3C0261:nseovm%3E2.0.co;2

Zhang, D.-L., & Fritsch, J. M. (1988b). A numerical investigation of a convectively generated, inertially stable, extratropical warm-core mesovortex over land. Part I: Structure and evolution. *Monthly Weather Review*, *116*(12), 2660–2687. https://doi.org/10.1175/1520-0493(1988)116%3C2660:anioac%3E2.0.co;2

Zhang, J., Howard, K., Langston, C., Vasiloff, S., Kaney, B., Arthur, A., … Dempsey, C. (2011). National mosaic and multi-sensor QPE (NMQ) system: Description, results, and future plans. *Bulletin of the American Meteorological Society*, *92*(10), 1321–1338. https://doi.org/10.1175/2011BAMS-D-11-00047.1

Zipser, E. J. (1969). The role of organized unsaturated convective downdrafts in the structure and rapid decay of an equatorial disturbance. *Journal of Applied Meteorology*, *8*(5), 799–814. https://doi.org/10.1175/1520-0450(1969)008%3C0799:troouc%3E2.0.co;2

Zipser, E. J. (1977). Mesoscale and convective-scale downdrafts as distinct components of squall-line structure. *Monthly Weather Review*, *105*(12), 1568–1589. https://doi.org/10.1175/1520-0493(1977)105%3C1568:MACDAD%3E2.0.CO;2

Zuluaga, M. D., & Houze, R. A. (2013). Evolution of the population of precipitating convective systems over the equatorial Indian Ocean in active phases of the Madden-Julian Oscillation. *Journal of the Atmospheric Sciences*, *70*(9), 2713–2725. https://doi.org/10.1175/Jas-D-12-0311.1